

**Special Collection:**

Trench migration, oroclinal bending and slab tearing: insight into geodynamics of convergent plate boundaries in 4D

**Key Points:**

- The Taraises Fm. preserves pre-, syn-, and post-folding magnetizations linked to Sevier thin-skinned tectonics
- Paleomagnetism reveals  $\sim 90^\circ$  counterclockwise rotation in the north and  $<30^\circ$  clockwise in the south of the Sierra Madre Oriental orocline
- The orocline formed by bending of an initially straight N-S fold-and-thrust belt between 66 and 55 Ma

**Supporting Information:**

Supporting Information may be found in the online version of this article.

**Correspondence to:**

D. Pastor-Galán,  
dpastorgalan@csic.es

**Citation:**

Guerra Roel, R., Chávez-Cabello, G., Aranda Gómez, J. J., Dekkers, M. J., Patiño Méndez, G., & Pastor-Galán, D. (2025). Bending the Sierra Madre Oriental: A Paleocene orocline. *Tectonics*, 44, e2025TC008856. <https://doi.org/10.1029/2025TC008856>

Received 29 JAN 2025

Accepted 28 OCT 2025

**Author Contributions:**

**Conceptualization:** Rafael Guerra Roel, Gabriel Chávez-Cabello, José Jorge Aranda Gómez

**Data curation:** Rafael Guerra Roel, Gerardo Patiño Méndez, Daniel Pastor-Galán

**Formal analysis:** Rafael Guerra Roel, Gabriel Chávez-Cabello, Mark J. Dekkers, Gerardo Patiño Méndez, Daniel Pastor-Galán

© 2025, The Author(s).

This is an open access article under the terms of the Creative Commons Attribution-NonCommercial License, which permits use, distribution and reproduction in any medium, provided the original work is properly cited and is not used for commercial purposes.

## Bending the Sierra Madre Oriental: A Paleocene Orocline

Rafael Guerra Roel<sup>1,2</sup> , Gabriel Chávez-Cabello<sup>3</sup> , José Jorge Aranda Gómez<sup>4</sup> , Mark J. Dekkers<sup>5</sup> , Gerardo Patiño Méndez<sup>3</sup> , and Daniel Pastor-Galán<sup>2,6,7</sup> 

<sup>1</sup>Posgrado de la Facultad de Ciencias de la Tierra. Carretera a Cerro Prieto Km 8, Universidad Autónoma de Nuevo León, Linares, México, <sup>2</sup>Universidad de Granada. Facultad de Ciencias de la Universidad de Granada. Campus Fuente Nueva, Granada, España, <sup>3</sup>Facultad de Ciencias de la Tierra. Carretera a Cerro Prieto Km 8, Universidad Autónoma de Nuevo León, Linares, México, <sup>4</sup>Universidad Nacional Autónoma de México, Centro de Geociencias, Juriquilla, México,

<sup>5</sup>Paleomagnetic Laboratory “Fort Hoofddijk”, Department of Earth Sciences, Utrecht University, Utrecht, The Netherlands,

<sup>6</sup>Consejo Superior de Investigaciones Científicas (CSIC), Madrid, España, <sup>7</sup>Frontier Research Institute for Interdisciplinary Science, Tohoku University, Sendai, Japan

**Abstract** The Sierra Madre Oriental belt of the Mexican thin-skinned fold-and-thrust belt, which formed during the Late Cretaceous due to the subduction of the Farallon Plate beneath North America, exhibits a pronounced curvature of approximately  $100^\circ$ , concave to the southwest. A recent paleomagnetic study in Jurassic rocks has classified the curvature of the Sierra Madre Oriental as an orocline. However, orocline formation remains loosely dated as syn-to post-orogenic, ranging from 120 to 50 Ma, which is the timing of the main deformation in the region. This poorly constrained kinematics prevented proposing a mechanism for the oroclinal bending, leaving both the tectonic driver and kinematics unresolved. In this study, we investigate the Cretaceous Taraises Formation along the curvature of the Sierra Madre Oriental Orocline to unravel its kinematics of formation. Our new paleomagnetic data set, along with joint-set analysis in 25 anticlines, allows for fold-tests and reveals pre-, syn-, and post-folding magnetizations that indicate  $\sim 90^\circ$  counterclockwise rotations with respect to the north, in the northern limb of the orocline and  $\sim 30^\circ$  clockwise rotations in its southern limb. Paleomagnetic data constrain the timing of the oroclinal bending to the Paleocene (66–55 Ma), which is later than the main thin-skinned folding event in the area.

**Plain Language Summary** The Sierra Madre Oriental in Mexico is a curved mountain range formed as a result of the subduction of the Pacific Ocean plates beneath North America. Its curve, about  $100^\circ$  wide and opening to the southwest, developed after the mountains were already built. Curves of this kind are known as oroclines. However, the exact timing and the process that created the orocline in northeast Mexico remain uncertain, with previous estimates ranging from 120 to 50 million years ago. To better understand its formation, we studied Cretaceous rocks across this curved region. We analyzed the magnetic signal preserved in the rocks together with fracture patterns in 25 folded structures. Our results show that the mountain belt rotated almost  $90^\circ$  to the left (counterclockwise) in the northern part of the orocline and about  $30^\circ$  to the right (clockwise) in the southern part. These rotations took place between 66 and 55 million years ago, during the Paleocene, and after the main folding event that shaped the range. Although the exact tectonic mechanism remains unclear, we suggest that subduction in eastern Mexico played the key role in driving the bending of the Sierra Madre Oriental.

### 1. Introduction

The North American Cordillera is one of the largest post-Paleozoic accretionary orogens, formed at a series of subduction zones that collectively accommodated plate convergence between Paleo-Pacific plates and seaways, and the North American Plate (Chen et al., 2025; DeCelles, 2004; Engebretson et al., 1985; Johnston, 2001; Sigloch & Mihalynuk, 2013; Torsvik et al., 2019; van der Meer et al., 2012). This orogen experienced protracted tectonic activity from the Mesozoic to the present day (e.g., DeCelles & Graham, 2015), often involving the closing of ocean basins of uncertain size and origin (e.g., Busby et al., 2023), the development of large strike-slip systems with poorly resolved displacements (e.g., Anderson et al., 2005; Housen and Beck, 1999), and associated large-scale oroclinal bending and buckling (Guerra Roel et al., 2024; Johnston, 2001). Unraveling the kinematic history of the Cordillera is crucial for understanding the tectonic and geodynamic processes operating in the East Pacific (e.g., Sigloch & Mihalynuk, 2017), exploring economic resources (e.g., Nokleberg et al., 2005), and understanding regional and global climate (Carruthers et al., 2024) through high-resolution paleogeographic

**Funding acquisition:** Rafael Guerra Roel, Gabriel Chávez-Cabello, José Jorge Aranda Gómez, Mark J. Dekkers, Daniel Pastor-Galán

**Investigation:** Rafael Guerra Roel, Gabriel Chávez-Cabello, Gerardo Patiño Méndez, Daniel Pastor-Galán

**Methodology:** Rafael Guerra Roel, Gabriel Chávez-Cabello, José Jorge Aranda Gómez, Mark J. Dekkers, Gerardo Patiño Méndez, Daniel Pastor-Galán

**Supervision:** Rafael Guerra Roel, Gabriel Chávez-Cabello, José Jorge Aranda Gómez, Mark J. Dekkers, Gerardo Patiño Méndez, Daniel Pastor-Galán

**Visualization:** Rafael Guerra Roel, Gabriel Chávez-Cabello, Daniel Pastor-Galán

**Writing – original draft:** Rafael Guerra Roel, Daniel Pastor-Galán

**Writing – review & editing:** Rafael Guerra Roel, Gabriel Chávez-Cabello, José Jorge Aranda Gómez, Mark J. Dekkers, Gerardo Patiño Méndez

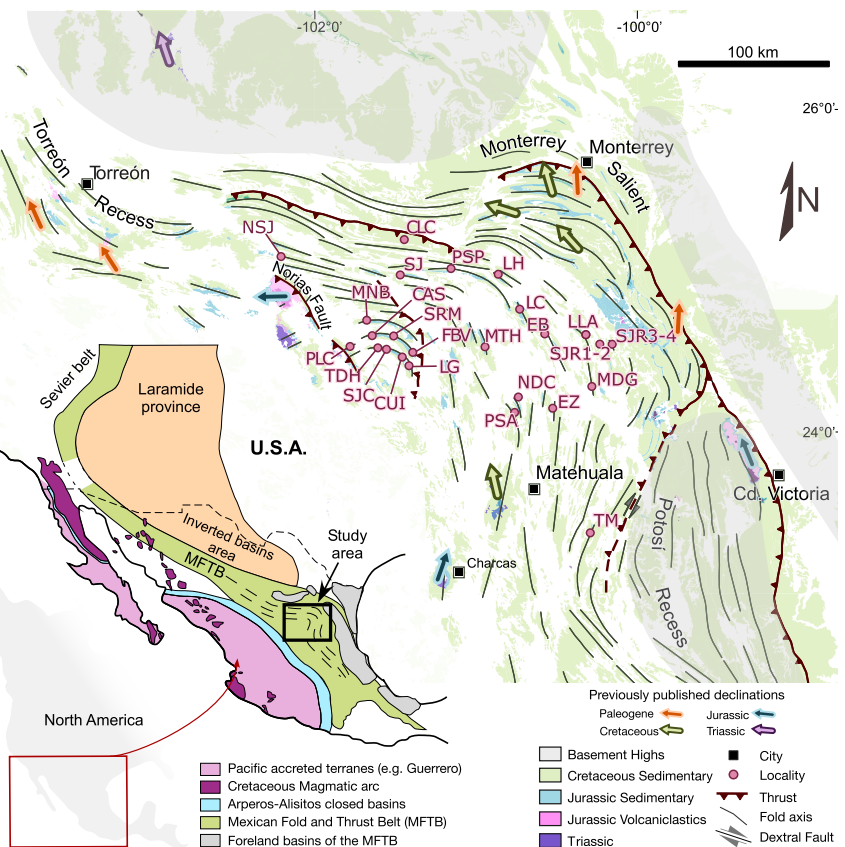


**Figure 1.** Regional structural map of the Sierra Madre Oriental Orocline. Note that folds (black lines) depict a curvature of  $\sim 110^\circ$ , the so-called Sierra Madre Oriental Orocline. The map shows previous paleomagnetic declinations (marked by arrows) and the localities of the studied anticlines.

reconstructions (Scotese et al., 2021). Quantifying the amount and timing of vertical axis rotations in the curved segments of the Cordillera (e.g., Weil et al., 2010; Yonkee & Weil, 2010) is essential for producing reliable kinematic reconstructions (example of a reconstruction accounting for vertical axis rotations: Sigloch & Mihalynuk, 2013).

The southern segment of the Cordillera, the Mexican Orogen, extends over 2,000 km from Sonora to Oaxaca (Figure 1; e.g., Campa & Coney, 1983; Fitz-Díaz et al., 2018; Martini et al., 2014; Suter, 1984, and references therein). Despite the extensive structural and geochronological knowledge of the orogen (e.g., Fitz-Díaz et al., 2014; Ramírez-Peña et al., 2019), several unresolved tectonic questions remain, such as the extent and displacement of alleged transforms (Mojave-Sonora megashear vs. California-Coahuila transform fault; e.g. Anderson et al., 2005), the origin and movement of the Guerrero terrane (e.g., Boschman et al., 2018; Busby & Centeno-García, 2022), and how and when the Sierra Madre Oriental Orocline formed (Guerra Roel et al., 2024). The Sierra Madre Oriental Orocline, a  $110^\circ$  bend in the trend of the Cordillera in NE Mexico marked by the curved trace of fold-axes, has largely unknown kinematics. Pioneering studies, such as those by Nemkin et al. (2019) on the Monterrey Salient and Guerra Roel et al. (2024) (Figure 1), demonstrated the existence of up to  $90^\circ$  counterclockwise vertical-axis rotations in Cretaceous and Jurassic rocks. Their data, however, could only constrain the timing of orocline formation to between 120 and 50 Ma.

Paleomagnetism is a key method for measuring when and where vertical-axis rotations occurred. By identifying their timing, it helps distinguish whether orogenic curvature was inherited from older crustal structures or formed later through tectonic processes (e.g., Eldrege et al., 1985; Maffione et al., 2013; Weil et al., 2016). However, it works best when accompanied by rock magnetism and detailed structural data, ensuring reliable interpretations of tectonic rotation histories (e.g., Weil et al., 2013; Yonkee et al., 2024; Yonkee & Weil, 2015). In the case of layer-parallel shortening fabrics, joints are typically the first structures to develop, and, in contrast to other structures,

they are consistently parallel at regional scales (Engelder & Geiser, 1980; Pastor-Galán et al., 2011). Thus, joint sets are the useful brittle structures for assessing vertical axis rotations. The primary objective of this paper is to precisely determine the kinematics of orocline formation in the Sierra Madre Oriental. To that end, we combine paleomagnetic and joint analysis from the limestones and marls of the Taraises Formation, an ideal formation due to its extensive outcrops along the orocline trend and its depositional age.

## 2. Geological Background

The North American Cordillera is a subduction driven orogenic system that extends from Alaska to Mexico (Fitz-Díaz et al., 2018; Johnston, 2001), resulting from the subduction of the Panthalassa-Pacific plates below the western margin of North America (e.g., Fuston & Wu, 2020; Yonkee et al., 2024; Yonkee & Weil, 2015). The style and distribution of deformation within the Cordilleran system have evolved over time due to changes in the absolute motion of the overriding North American plate relative to the Farallon and Kula plates, and the nature of the subducting lithosphere (e.g., Torsvik et al., 2019; Wright et al., 2016). The hypotheses explaining such changes include variations in the age of the oceanic crust, the presence of oceanic plateaus, and the accretion of terranes (e.g., Dickinson, 2004; Yonkee & Weil, 2015). The subduction process and the consequent loss of oceanic spreading records introduce significant uncertainties in reconstructing the Mesozoic plate-tectonic configuration of the northeast Pacific. Specifically, the continuous loss of seafloor makes it difficult to determine the number of intervening oceanic plates (Boschman et al., 2018) despite the efforts in recovering them from tomography (Chen et al., 2025).

The North American Cordillera is constructed of a forearc accretionary complex, a magmatic arc, a retroarc hinterland, a fold-and-thrust belt (the so-called Sevier), and a foreland basin shaped by thick-skinned tectonics (known as Laramide; e.g., Weil & Yonkee, 2023; Yonkee & Weil, 2015, and references therein). In addition to the subduction and accretion of allochthonous terranes, the orogenic architecture in the Cordillera is partially attributed to the distribution of the North American basement (e.g., Martini & Ortega-Gutiérrez, 2018; Yonkee et al., 2024). In the USA, the post-Rodinia rifted Laurentian craton margin had significant control on the structural evolution of both the Sevier and Laramide belts and their resulting geometry (DeCelles, 2004; Lawton, 1994; Weil & Yonkee, 2012). In contrast, the southern margin of the North American plate in Mexico, has basement rocks that define a series of mobile blocks of Laurentian, Gondwanan and Pacific origins (Campa & Coney, 1983; Centeno-García, 2017; Dickinson & Lawton, 2001; Keppie, 2004; Sedlock et al., 1993) located between the southern edge of Laurentia and the northwest edge of Gondwana during the Paleozoic assembly of Pangea (e.g., Domeier & Torsvik, 2014; Pastor-Galán, 2022). The Triassic to Jurassic breakup of Pangea and subsequent plate reorganization (e.g., Müller et al., 2019), facilitated the development of Mesozoic extensional to transtensional basins and carbonate platforms on fault-bounded basement highs. These features are now part of both a Sevier thin-skinned fold-and-thrust belt with localized Laramide thick-skinned structures (Fitz-Díaz et al., 2018; Ramírez-Peña et al., 2019; Weil & Yonkee, 2023).

In Mexico, the Paleo-Pacific subduction led to the accretion of the Guerrero Terrane around 115 Ma, which triggered the initial shortening phase of the Mexican orogen (Centeno-García et al., 2008; Fitz-Díaz et al., 2018; Martini et al., 2013). Although it is unknown how far the Guerrero terrane drifted from the Mexican mainland, some suggest that oceanic crust (the Mezcalera plate) developed in between them (Dickinson & Lawton, 2001; Martini et al., 2011). During the Albian, Guerrero rocks were thrust eastwards over a back-arc, triggering the development of a regional suture in western Mexico (Centeno-García et al., 2008; Martini et al., 2013). The Mexican Fold-and-Thrust Belt (MFTB; thin-skinned defined as “Sevier-style” onwards), and different foreland basins developed during diachronic shortening from west to east when flat slab subduction of the Farallon plate initiated (Upper Cretaceous-Early Eocene; Fitz-Díaz et al., 2018 and references therein). During the Paleocene-Eocene, thick-skinned structures formed in the MFTB (Chávez-Cabello et al., 2005; Ramírez-Peña et al., 2019; Zhou et al., 2006). These Laramide structures are thought to result of basement fault reactivation during the late stage of flat-slab subduction (Weil & Yonkee, 2023 and references therein). In Mexico, the subduction of an oceanic plateau (Liu et al., 2010) or the increased westward motion rate of the North American plate during the Paleogene (van der Meer et al., 2012) has also been invoked for the origin of the thick-skinned tectonic event.

The stratigraphy of the Mexican orogen consists of two main tectonostratigraphic assemblages: (a) a thick succession of deep-water marine strata overlying mafic volcanic rocks deposited in one or more offshore basins before the accretion of the Guerrero Terrane (Aptian), and (b) synorogenic strata deposited in foreland basins

adjacent to the orogenic wedge. The basement of Mexico consists of Precambrian–Paleozoic rocks interpreted as Pangea-derived blocks dispersed across Mexico (Keppie & Ortega-Gutiérrez, 2010). In the Late Triassic to Early Jurassic, extensional tectonics created fault-bounded basins where horsts hosted carbonate platforms, while grabens accumulated deeper marine deposits in the Cretaceous (e.g., Busby & Centeno-García, 2022; Eguiluz et al., 2000). Subduction continued along the western margin through the Mesozoic, interrupted briefly during the Early Jurassic (Parolari et al., 2022). From the beginning of the Jurassic to the Bathonian, several volcano-clastic successions were deposited in structural grabens along the Paleo-Pacific western margin of Mexico, whose origin remains debated (cf. Busby & Centeno-García, 2022). From the Late Jurassic to Early Cretaceous, drifting associated with the breakup of Pangea and rollback of the Paleo-Pacific plates led to the formation of several marine basins, including the Arperos Basin and the Mesozoic Basin of Central Mexico (e.g., Martini & Ortega-Gutiérrez, 2018). In the Early Cretaceous, the region experienced continuous subsidence, leading to the deposition of over 2,000 m of shelf carbonates, a sedimentary environment partially controlled by the Coahuila, Tamaulipas, and Valles–San Luis Potosí basement highs (e.g., Eguiluz et al., 2000; Goldhammer, 1999). Platform sedimentation continued until the Albian, where the first signs of tectonic instability (such as breccias, disharmonic folds, and faults) occurred concomitantly with angular unconformities in the Arperos Basin, suggesting active deformation (Guerra Roel, 2019). These rocks predate the “Sevier” shortening phase in the Mexican orogen and were subsequently thrust over the continental margin, forming a highly deformed suture zone between the Guerrero terrane and Late Paleozoic to Mesozoic rocks flanking the Mesoproterozoic core of eastern Mexico (e.g., Martini et al., 2014).

The second assemblage, deposited adjacent to the orogenic wedge after Guerrero's accretion, is known as the foreland basin fill (Fitz-Díaz et al., 2018; Martini & Ortega-Gutiérrez, 2018). Following deposition of the carbonate platforms, the foreland had dominantly turbiditic sedimentation. This sedimentation was diachronous from west to east, reflecting progressive eastward migration of the tectonic wedge into the foredeep, continuing until Maastrichtian times (Ocampo-Díaz et al., 2016).

## 2.1. The Sierra Madre Oriental Orocline

The Sierra Madre Oriental is part of the MFTB and is partly intruded and overlain by rocks of the Sierra Madre Occidental and the Trans-Mexican Volcanic Belt. The Sierra Madre Oriental is located in the northeastern section of the MFTB (Figure 1). This part of the belt forms a sinuous band dominated by folds and thrusts, with four major curvatures: the Torreón recess, the Potosí recess, the Monterrey salient, and the Concepción del Oro salient (Figure 1). These curvatures may reflect the original coastline geometry and the geographic distribution of basement highs, although this has not yet been determined (e.g., Nemkin et al., 2019). In general, aside from the Torreón recess, the other curvatures mentioned above appear to represent local features or parasitic curvatures superimposed on the main regional curvature (Figure 1).

In northeast Mexico, regional structures associated with the “Sevier” shortening phase are dominated primarily by symmetrical, overturned, detachment-, fault-bend-, and fault-propagation folds, listed here in order of decreasing frequency (e.g., Ramírez-Peña & Chávez-Cabello, 2017). The style of contractional deformation is predominantly thin-skinned, characterized by folds and thrusts that developed over a regional décollement (Pfiffner, 2006, 2017). Along the trace of the Mexican Fold and Thrust Belt, exposures of Jurassic volcano-sedimentary strata and Paleozoic metamorphic rocks are rare. Where present, they are usually exposed by high-angle reverse faults that cut older folds vertically or appear in the cores of antiforms (Eguiluz et al., 2000; Fitz-Díaz et al., 2018; Guerra Roel, 2019; Ramírez-Peña & Chávez-Cabello, 2017; Ramírez-Peña et al., 2019; Williams et al., 2021; Zavalá-Monsiváis et al., 2012). In Concepción del Oro (East of the Norias Fault on Figure 1), high-angle reverse faults crosscut and rotate andesitic lavas ( $40.7 \pm 0.6$  Ma; U-Pb zircon) and Late Eocene conglomerates, suggesting younger faulting unrelated to regional thin-skinned deformation (Ramírez-Peña et al., 2019).

Previous paleomagnetic studies revealed vertical-axis fold rotations (clockwise and counterclockwise) during shortening, indicative of oroclinal bending or buckling between 120 and 50 Ma (Guerra Roel et al., 2024, and references therein). Contrasting deformation styles differentiate basinal and marine shelf environments within the Sierra Madre Oriental (Eguiluz et al., 2000; Fitz-Díaz et al., 2018; Padilla y Sánchez, 1985). Contractual deformation in the MFTB was diachronous, progressing from west to east between 93 and 43 Ma, as constrained by Ar-Ar dating of authigenic illite on cleavages (Fitz-Díaz et al., 2014) and shear zones (Fitz-Díaz et al., 2016), U-Pb zircon dating of syn-tectonic granitoids (Ramírez-Peña & Chávez-Cabello, 2017), biostratigraphic analyses



**Figure 2.** Examples of sampled localities in the Taraises formation. (a) shows an overview of an outcrop and (b) a detailed description of the sampled sections including lines showing joint sets. (c) shows another section showing the joint sets. In all three, hammer for scale. (d) shows a pyritized ammonite from the Taraises Formation that was subsequently oxidized.

of syn-orogenic sediments (Juárez-Arriaga et al., 2022; Ocampo-Díaz et al., 2016), and thermochronological studies of uplifted blocks such as Real de Catorce and El Potosí (Gutiérrez-Navarro et al., 2021; Williams et al., 2021). In the sampled area, folding occurred between 93 Ma (core of the curvature) and 66 Ma (outermost area of the curvature) (Fitz-Díaz et al., 2018).

## 2.2. The Taraises Formation

The Taraises Formation (Figure 2), a Lower Cretaceous carbonate unit in northeastern Mexico, is regionally distributed across the Sierra Madre Oriental and the Coahuila Block (Blauser & McNulty, 1981). This formation unconformably overlies the Upper Jurassic La Casita and La Caja formations and transitions upward into the Tamaulipas and Cupido formations (Goldhammer & Johnson, 2001; Michalzik, 1988; Ocampo-Díaz et al., 2016; Ramírez-Peña & Chávez-Cabello, 2017). Lithologically, it comprises fossiliferous limestone, calcareous shale, and subordinate dolostone, reflecting deposition in shallow to mid-ramp marine environments (Blauser & McNulty, 1981; Imlay, 1936). Thickness varies from approximately 60 m to over 665 m, with facies changes attributed to synsedimentary tectonic activity related to the Coahuila Block and regional basin evolution (Blauser & McNulty, 1981). The unit's stratigraphy is marked by ammonite-rich intervals and calpionellid biozones, which provide critical biostratigraphic markers for regional correlations (Blauser & McNulty, 1981; Imlay, 1936). Deposition of the Taraises Formation occurred during a period of widespread marine transgression following Late Jurassic rifting, with carbonate productivity influenced by intra-platform shoals, reefal complexes, and pelagic influxes (e.g., Suter, 1990). Paleoenvironmental reconstructions suggest fluctuating water depths, evidenced by cyclic alternations of laminated lime mudstones, indicative of low-energy settings, and bioturbated packstones with benthic foraminifera, which reflect higher-energy conditions (Blauser & McNulty, 1981).

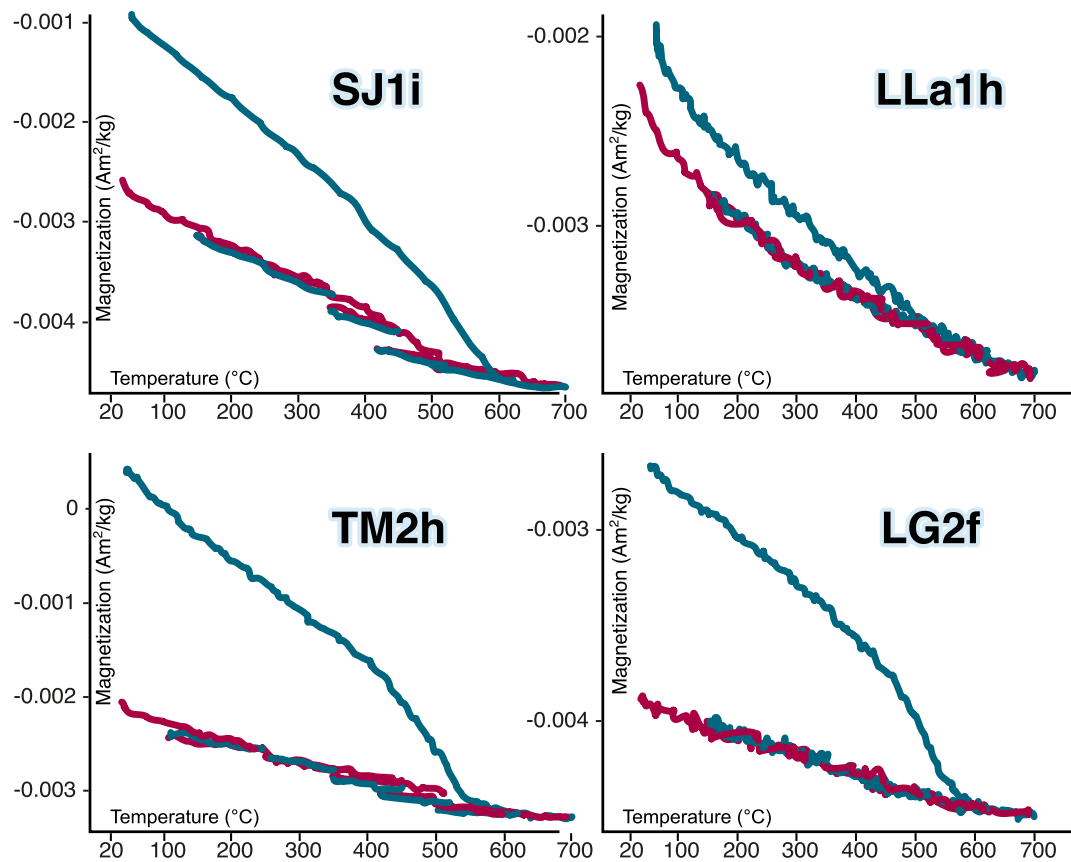


**Figure 3.** Magnetization versus temperature runs. The Curie balance runs show a progressively lowering magnetization on heating, denoting (Ti)-magnetite as the main magnetic carrier, evidenced by a small drop in magnetization at temperatures of 480–520°C. Note that all numbers are negative. This implies that there is no holder correction performed (unavailable in the software at the time of processing).

### 3. Methods and Results

#### 3.1. Sampling Strategy

We collected a total of 671 cores for paleomagnetism using a petrol engine drill from 25 anticlines in the Taraises Formation (Figure 2) following the trace of the Sierra Madre Oriental Orocline. We chose anticlines where plunging axes were close to 0°. We sampled ~13 cores at different stratigraphic levels in marls sequences in each limb of all 25 anticlines, defining two localities per anticline for subsequent fold-tests. In addition, we took ~30 joint measurements in each locality (see Engelder & Geiser, 1980; Pastor-Galán et al., 2011), making a total of more than 1,200 measurements (see Data Set S1). We chose the Taraises Formation since its broad distribution and timing of deposition and deformation are optimal to constrain the Sierra Madre Oriental Orocline's kinematics. Localities were coded as acronyms from their anticline name, followed by a number that indicates the limb (Data Set S1; Figure 1).

#### 3.2. Paleomagnetism and Rock Magnetism

We conducted five thermomagnetic runs to determine the optimal demagnetization procedures (Figure 3). We used the modified horizontal translation-type Curie balance from the Paleomagnetic Laboratory Fort Hoofddijk, Utrecht University, Netherlands (Mullender et al., 1993). Runs included heating and cooling cycles to progressively higher temperatures in each heating step to distinguish between thermochemical alteration and genuine magnetic behavior. Heating cycles increased in steps of 200°C and with intermittent cooling of 100°C. Thermomagnetic curves revealed that samples contained minor (Ti)-magnetite, which is the magnetic carrier, evinced by the step in magnetization around 500°C, which is particularly visible in SJ1i, less so in TM2h and LG2f and subtle in LLa1h (Figure 3).

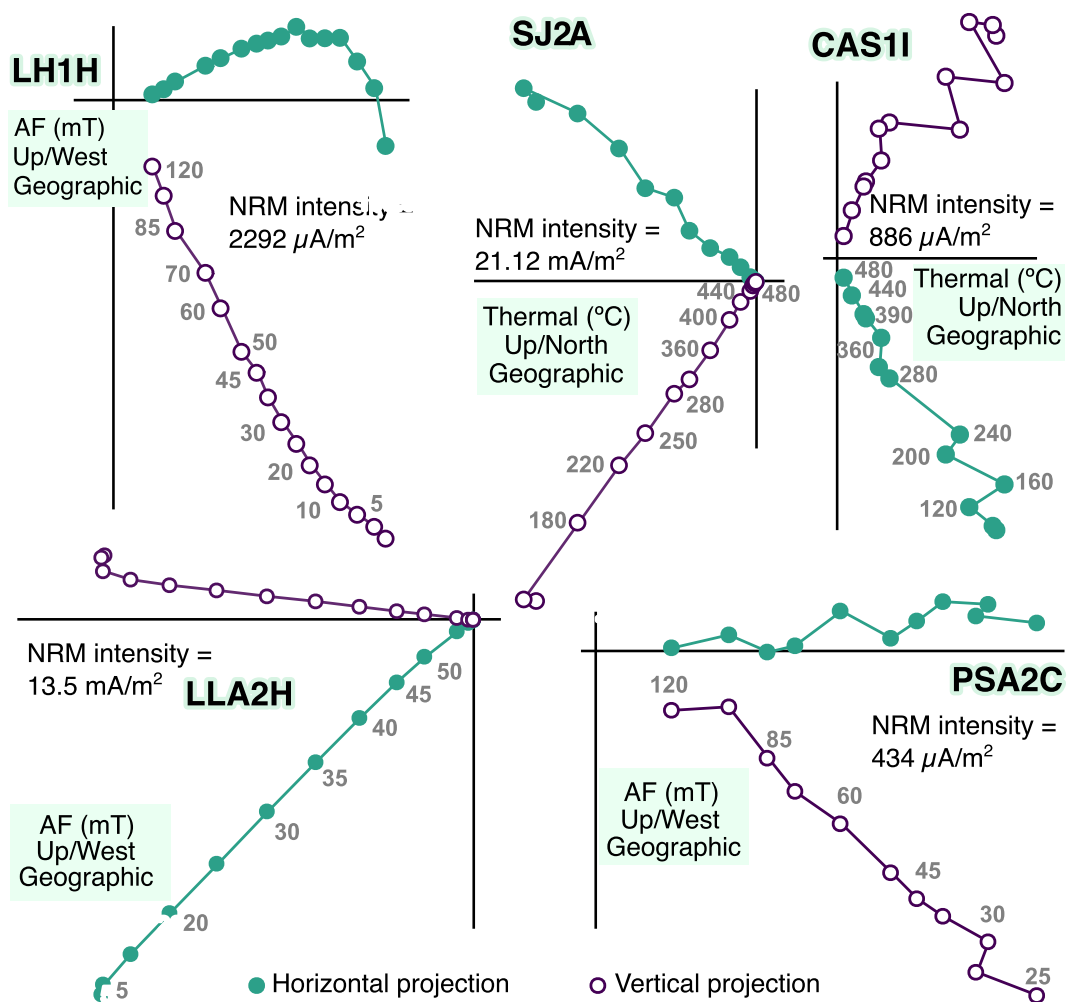


**Figure 4.** Selected Zijderveld diagrams (Zijderveld, 1967) of five representative samples. All samples show a single ChRM component that demagnetizes to the origin (Thermal and AF). AF demagnetization was preceded by thermal demagnetization at 150°C (van Velzen & Zijderveld, 1995). LH1H shows the presence of a viscous component that was removed at low coercivities (<15 mT) and temperatures (<200°C). Closed and open circles indicate declination and projection of the inclination respectively.

Paleomagnetic cores were cut into 2.2 cm standard specimens. We investigated the samples' magnetic remanence using thermal and alternating field (AF) demagnetization. We conducted stepwise thermal demagnetization in 20–100°C increments until complete demagnetization in 200 samples (Figure 4). We performed AF demagnetization with a robotic 2G-SQUID magnetometer, applying variable field increments (4–10 mT) up to 100 or 120 mT (Mullender et al., 2016) in the rest of them (471). Since high-coercivity, low-blocking temperature minerals (goethite) or alteration rims due to partial oxidation of magnetite are often found in marls and limestones, we coupled the AF demagnetization with pre-heating to 150°C in the thermal demagnetizer (van Velzen & Zijderveld, 1995). To calculate magnetic component directions from "Zijderveld" vector end-point demagnetization diagrams, we used the open-source software "Paleomagnetism.org" (Koymans et al., 2016, 2020) for principal component analysis (Kirschvink, 1980). Specimens' characteristic remanent magnetization (ChRM) directions from at least five consecutive demagnetization steps and with a maximum angular deviation (MAD) <15° when not anchored to the origin (McElhinny & McFadden, 1999) were considered meaningful directions. We also used the McFadden and McElhinny (1988) method of combining great circles and best-fitted set point directions for samples where components were difficult to isolate (performed in only 13 out of 671 cases). From the 671 sampled cores, 608 delivered an interpretable ChRM. We applied a 45° cut-off for the data set of each locality to discard outlying data points; 41 directions were not considered further.

We evaluated mean directions (Table S1 in Supporting Information S1) using Fisher statistics of virtual geomagnetic poles (VGPs) corresponding to the isolated ChRM directions. In some samples, a viscous magnetic component was removed at low coercivities or temperatures ( $<15$  mT and  $<200^\circ\text{C}$  respectively; Figure 4). However, we could not determine the origin or orientation of this viscous component. In a few localities, we retrieved a medium temperature and coercivity component ( $200\text{--}400^\circ\text{C}$  and  $8\text{--}30$  mT), that was statistically significant in only 5 localities (7 or more directions; CAS1, CUI1, FBV2, NSJ1, PLC1, Table S1 in Supporting Information S1). The medium temperature and coercivity directions do not concentrate nor concur with the expected inclinations. We have no means to test the potential structural corrections because we did not find this component in both limbs of any anticline. In addition, there is no similarity between components in geographic or tectonic coordinates. Therefore, we cannot retrieve a faithful paleomagnetic direction from this component. (Titano-)magnetite is the dominant magnetic carrier of the ChRM in all samples as evidenced by maximum unblocking temperatures of  $480\text{--}520^\circ\text{C}$  and alternating magnetic fields of  $60\text{--}90$  mT (Figure 4). Whereas the majority of the samples (553/608) decay straight to or close to the origin (Figure 4), some samples analyzed with AF did not (55/608). It was impossible to recover any further component since the demagnetization behavior became erratic from 60 mT upward. All localities show single polarity ChRM. In geographic coordinates, the ChRM component ranges from west to northeast and points down in all cases but 3 (MDG1, MTH2, SRM2; Table S1 in Supporting Information S1). One of the studied anticline limbs (SRM2, Table S1 in Supporting Information S1) did not deliver enough meaningful directions ( $n = 4$ ), and has not been considered for further analysis.

To assess the quality and reliability of the ChRM distributions, we applied the N-dependent A95 envelope of Deenen et al. (2011). This criterion determines whether the scatter of VGPs in a locality is consistent with paleosecular variation (PSV) of the geomagnetic field ( $\text{A95min} \leq \text{A95} \leq \text{A95max}$ ). Most localities provided values of scatter consistent with the PSV (20/25). Four localities (LG1; PLC2; SJC1; SJR1) show parameters consistent with a spot reading of the magnetic field ( $\text{A95} < \text{A95min}$ ). We tested these limbs at the anticline scale. When combined with their corresponding limbs, their statistical parameters remain acceptable and can still provide information on vertical-axis rotations. Therefore, we decided to keep those localities for further analysis. One locality (SRM2) shows a large scatter (dispersion parameter ( $k$ ) = 6, and  $\text{A95} > \text{A95max}$ ), which precludes a reliable fold-test. Since we cannot precisely know the adequate structural correction for that locality, the SRM anticline was discarded for further analysis. Table S1 in Supporting Information S1 contains the statistical synthesis of each locality. The raw and interpreted data at specimen level can be accessed in the repositories of [Paleomagnetism.org](#), and Zenodo (see links in the Data Availability Statement).

We performed 24 fold-tests in total (Tauxe & Watson, 1994; Figures 5–7) to establish the relative age of the ChRM. The results are summarized in Table 1. The fold tests indicate the presence of pre-folding (Figure 5), post-folding (Figure 6), and perhaps, syn-folding (Figure 7) magnetizations (Table 1). One anticline (MTH) yielded an inconclusive fold-test, as the declinations of each flank did not concentrate at any point during the fold-test (from  $-150\%$  to  $+150\%$  correction) and was therefore not considered for further analysis. Three fold-tests produced two maximum concentrations (tau maxima) in both geographic and tilt-corrected coordinates (LH, MDG, and SJR3-4; Table 1; Figures 5 and 6). In the cases of MDG and SJR3-4, the fold test generated an artificial tau maximum before untilting (geographic coordinates), where directions are close to antipodal. However, these directions are in the same hemisphere (both pointing down), not opposite, and the inclinations before untilting are too shallow (around  $\sim 0^\circ$ ) to represent a post-folding magnetization (Late Cretaceous or younger): Mexico then was at a similar latitude as today (Vaes et al., 2023). The case of LH is the opposite: after tilt correction, two close-to-antipodal but same-hemisphere shallow inclinations produce a high tau. However, in geographic coordinates, it fits well with a Cretaceous inclination. If we consider the paleomagnetic directions with minimal dispersion the best fit of each fold-test (i.e., geographic, fully tilt corrected, or with a given percentage of unfolding), all localities present single polarity, down directed inclinations and W to NE declinations (Figure 8). Only the NSJ anticline shows two polarities (Figure 8). The average inclination of the pre-folding localities and the syn- and post-folding ones with inclination only statistics (Arason & Levi, 2010) yield an average pre-folding inclination of  $44.6^\circ \pm 5^\circ$  and a slightly higher syn- and post-folding inclination of  $46.4^\circ \pm 2^\circ$  (Figure 9). When compared with the Global Apparent Polar Wander Path (GAPWaP, Vaes et al., 2023) these inclinations are consistent with a primary (145–130 Ma for the Taraíses Fm.) magnetization for the pre-folding cases and 90 to 55 Ma for the syn- and post-folding.

To quantify the potential vertical axis rotations associated with the Sierra Madre Oriental Orocline, we used the declination of each anticline in: (a) geographic coordinates for sites with a negative fold-test (CAS, FBV, LG, LH, LLA, MNB, NDC, PLC, PSA, SJ, SJC, TDH); (b) the tilt corrected declination in the cases of a positive fold-test

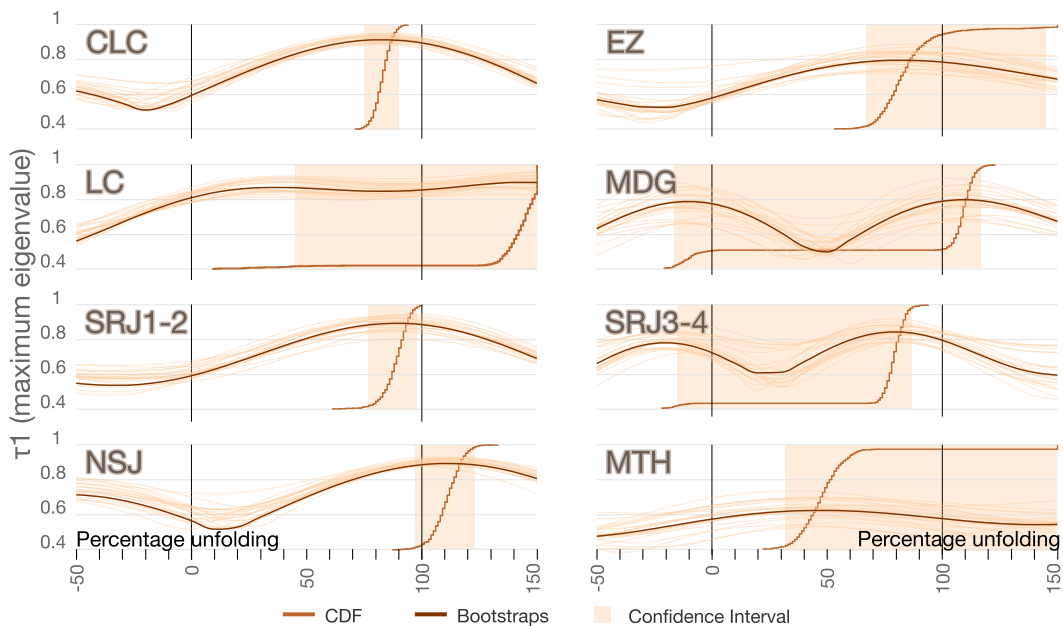


**Figure 5.** The eight anticlines that show a positive fold test (Tauxe & Watson, 1994). MDG and SJR3-4 show two tau maxima before and after untilting. However, this result is an artifact in geographic coordinates (see text).

(CLC, EZ, LC, MDG, SJR1-2, SJR3-4, NSJ); and (c) the declination corresponding to the tightest grouping in the case of syn-folding remagnetizations (CUI, PSP, TM, EB). The observed declinations approximately follow the trend of the orocline regardless of their magnetization timing, with anticline NSJ (perpendicular to the trend) as the only exception (Figure 10; Table 1; Table S2 in Supporting Information S1). In the studied area, post-folding remagnetization is more prevalent in the core of the orocline, while pre-folding magnetization occurs more frequently along its outer arc. We used a declination of  $345^\circ$  as a reference to calculate rotations since the North American plate was stable during the interval from 140 to 50 Ma (Vaes et al., 2023).

### 3.3. Anisotropy of the Magnetic Susceptibility

Anisotropy of magnetic susceptibility (AMS) measures the induced magnetization in a rock in a small magnetic field applied in different directions (e.g., Parés, 2015). The results are represented as a triaxial ellipsoid whose shape depends on the crystallographic preferred orientation of minerals, their grain size, shape, and alignment. AMS can be used as a proxy for identifying weak rock fabrics that are not evident through other techniques. AMS can also be a good indicator of potential anisotropies of the remanence due to deformation (Borradaile & Jackson, 2010). We measured the AMS fabric in 348 samples ( $\sim 14$  per anticline) using an AGICO MFK1-FA susceptometer (nominal sensitivity  $2 \times 10^{-8}$  SI). The results are shown in Figure S1 of Supporting Information S1. All sites show very low degrees of anisotropy ( $P < 1.05$ ), and the AMS ellipsoids have poorly defined axes with very large uncertainties, which preclude a straightforward interpretation of the data sets in terms of sedimentary or structural fabric. We argue that the poorly defined locality-wise fabrics are the result of sample-level individual axis directions that are not statistically well defined. 80% of samples show *F*-test values lower than reference (3.5), which means that they are most likely isotropic (Jelínek, 1977). Considering such results, we are not further interpreting the AMS results in terms of fold-and-thrust belt kinematics.

### 3.4. Joint Analysis

Analysis of regional joint sets that preserve a record of the far-field tectonic stress field (e.g., Engelder & Geiser, 1980; Gross et al., 1995), which is geometrically dependent on plate boundaries (e.g., Heidbach et al., 2007), combined with paleomagnetic data, provide a robust method to estimate vertical-axis rotations. They provide arguably one of the best records of the stress field during deformation in brittle structures. In this sense, complicated joint-set systems are the response to a tangled stress history rather than a complicated non-parallel stress field. Joints typically develop within the  $\sigma_1-\sigma_2$  plane, which in previously undeformed contractional

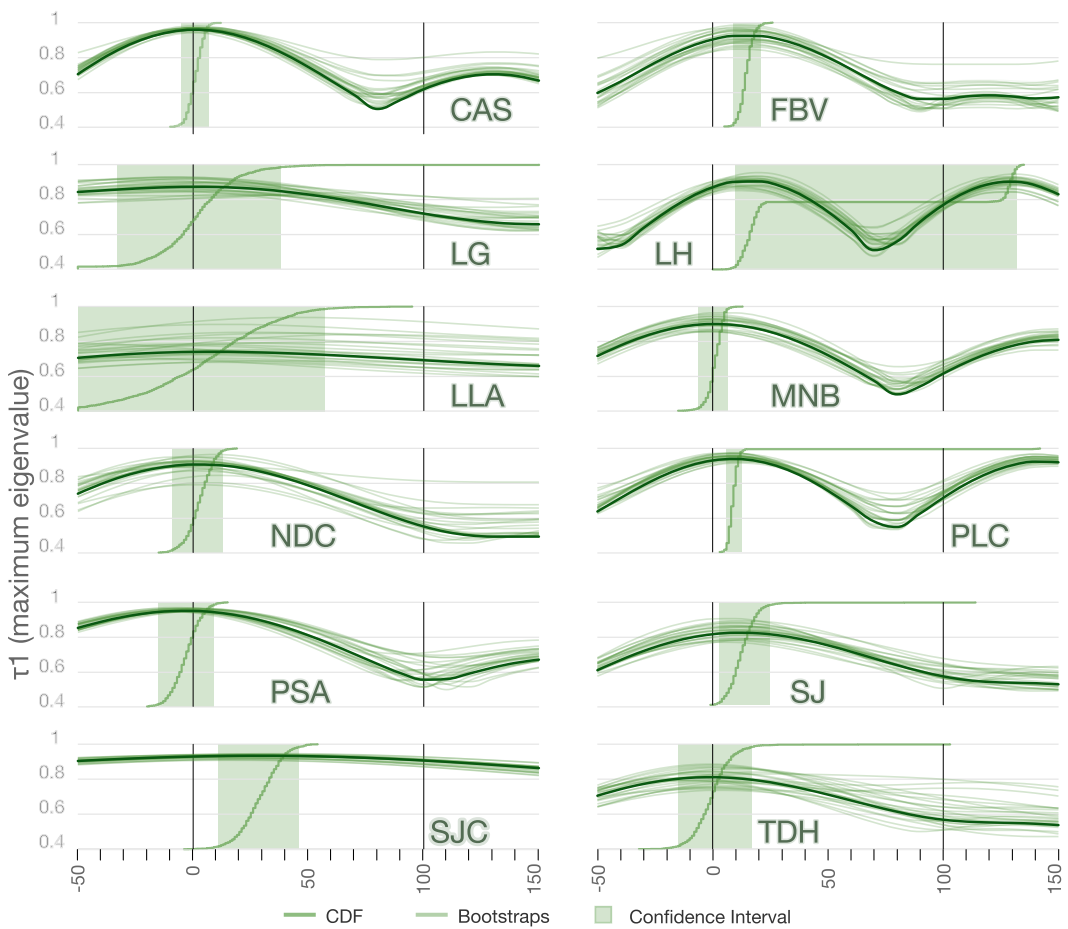


**Figure 6.** The 12 anticlines that show a negative fold test (Tauxe & Watson, 1994). Note: LH shows two maxima; however, we deem the post-tilting distribution unreliable (see text for details).

settings is roughly normal to the axis of the folds that accommodate the shortening (Engelder & Geiser, 1980; Whitaker & Engelder, 2005). Since far-field tectonic stress is close to rectilinear at regional scales (Heidbach et al., 2007), the presence of joint sets with regional curved patterns are most likely related to subsequent vertical axis rotations (e.g., Pastor-Galán et al., 2011). This feature makes joint patterns an effective tool for studying the kinematics and structural evolution of curved orogens (e.g., Pastor-Galán et al., 2011, 2014; Whitaker & Engelder, 2006; Yonkee & Weil, 2010).

We analyzed the spatial distribution of systematic joint sets from the 23 anticlines that provided significant fold-tests to constrain possible vertical-axis rotations (~60 readings per anticline). Joints in the Taraises Formation show no apparent slip indicators, suggesting they originated as Mode I (tensile) fractures that were not reactivated. We did not consider joint set orientations that represent less than 4% of the total measured population. In most cases (20), we identified a vertical and strike-perpendicular (“cross-fold”) joint set, which is typical in fold-and-thrust belts (e.g., Hancock, 1985). We identified a strike-parallel set in 3 localities (Figure S2 in Supporting Information S1), which is insufficient for kinematic analyses (e.g., Engelder & Geiser, 1980). Due to their geometric characteristics (vertical and perpendicular to the fold axis), back-tilting the joint sets did not offer any benefit. The strike-perpendicular joint set draws a fan pattern perpendicular to the trend of the Sierra Madre Oriental Orocline in the Cretaceous basin (Figure 10; Figure S2 in Supporting Information S1).

### 3.5. Orocline Test

The orocline test (see Pastor-Galán et al., 2017; Yonkee & Weil, 2010) compares the strike ( $S$ ) of the orogen with the orientation of a given fabric (e.g., paleomagnetic declinations or joint sets) in a Cartesian coordinate system.

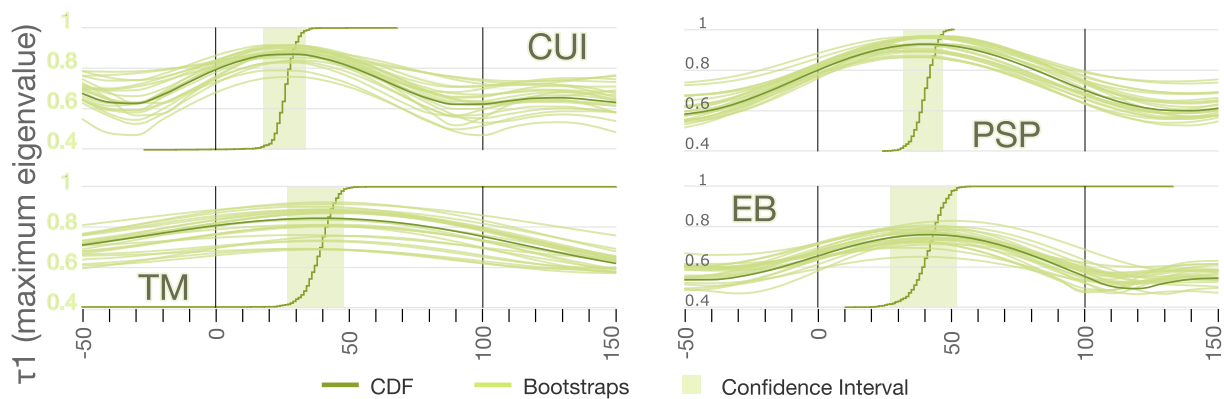


**Figure 7.** All four syn-folding fold tests (Tauxe & Watson, 1994).

**Table 1**  
*Summary of Fold Test Results*

Collection	Foldtest	Coordinates						
		Range (%)	Dec	ΔDx	Strike	Lat.	Long.	
CAS	Negative	-5.00	7	295.26	8.15	255	24.6	-101.7
FBV	Negative	9.00	21	297.48	5.5	317	24.5	-101.4
LG	Negative	-40.00	36	35.56	5.57	8	24.4	-101.4
LH	Negative (1)	10.00	130	308.21	24.29	319	25.0	-100.9
LLA	Negative	-50.00	50	336.16	16.85	325	24.6	-100.3
MNB	Negative	-6.00	7	272.97	7.92	274	24.7	-101.7
NDC	Negative	-9.00	13	0.16	8.51	345	24.2	-100.7
PLC	Negative	6.00	13	292.96	5.75	239	24.5	-101.8
PSA	Negative	-15.00	9	2.42	6.16	336	24.1	-100.8
SJ	Negative	3.00	25	288.14	8.03	265	25.0	-101.5
SJC	Negative (2)	11.00	46	305.07	5.31	320	24.4	-101.5
TDH	Negative	-15.00	17	312.27	8.19	269	24.5	-101.6
CUI	Negative (Syn-30%)	19.00	34	328.32	6.97	284	24.5	-101.6
PSP	Negative (Syn-40%)	32.00	47	281.34	4.87	273	25.0	-101.2
TM	Negative (Syn-40%)	27.00	48	9.61	8.87	10	23.4	-100.3
EB	Negative (Syn-40%)	27.00	51	335.94	7.42	340	24.6	-100.6
CLC	Positive	75.00	90	302.86	6.51	282	25.2	-101.4
EZ	Positive	67.00	144	27.02	7.1	25	24.1	-100.5
LC	Positive (3)	39.00	150	329.55	7.09	318	24.7	-100.7
MDG	Positive (4)	-16.00	117	330.06	10.75	356	24.3	-100.3
SJR1-2	Positive	77.00	98	6.92	7.85	343	24.6	-100.2
SJR3-4	Positive	-15.00	87	8.11	12.51	350	24.5	-100.2
NSJ <sup>a</sup>	Positive	97.00	123	356.21	7.57	281	25.1	-102.2

*Note.* ΔDx uncertainty in Declination (1) Foltest generates artificially two peaks because the directions get closer to antipodal, but with the same inclination not opposite. (2) Foldtest looks non-conclusive but  $k$  is better in Geo. (3)  $k$  and K concentrate better in TC. (4) Foldtest generates artificially two peaks because the directions in geo are near to antipodal but with the same inclination not opposite. <sup>a</sup>It is the only site that does not follow the pattern and we consider it an outlier.

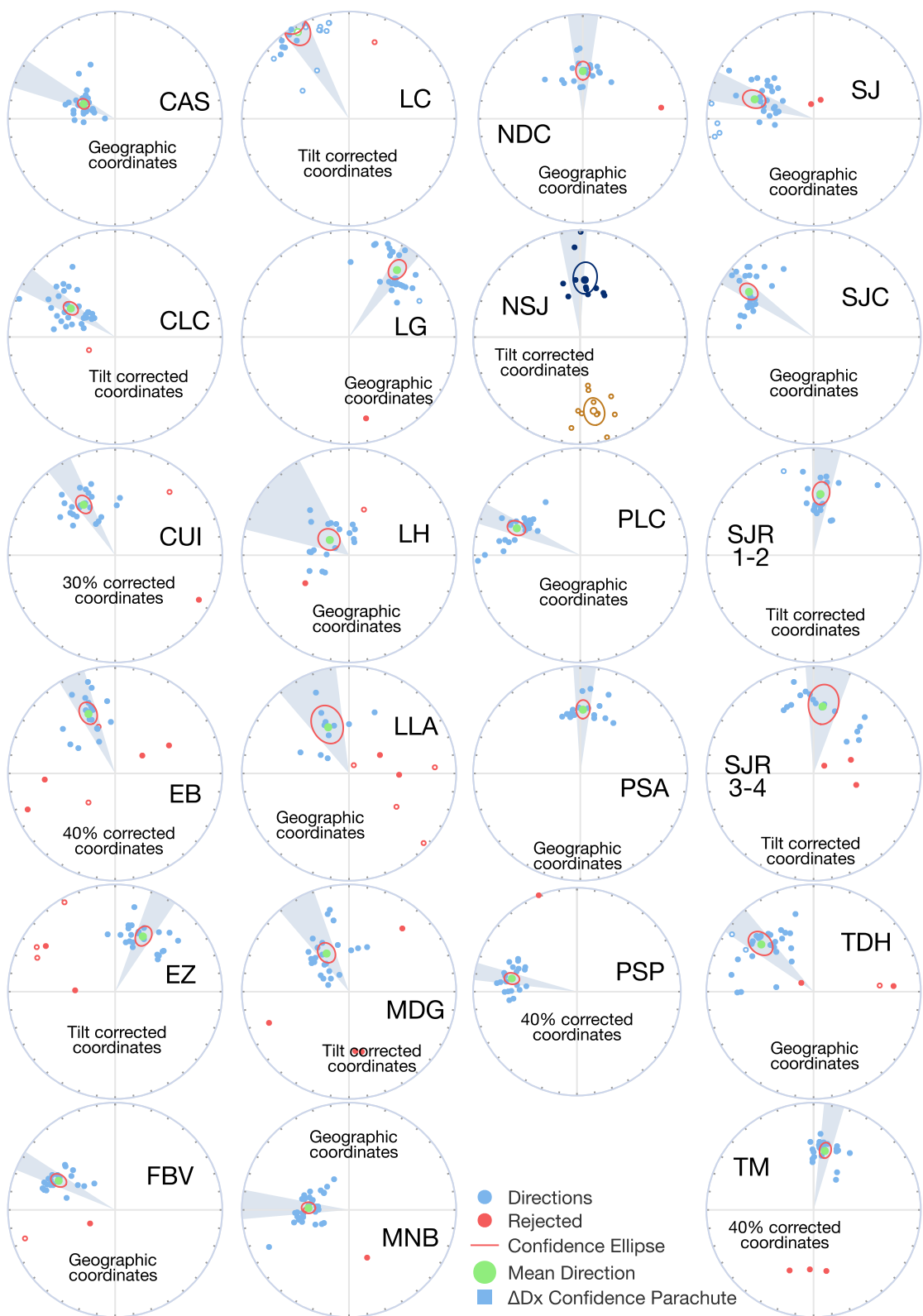


**Figure 8.** Paleomagnetic directions of each anticline with the best-fit unfolding correction.

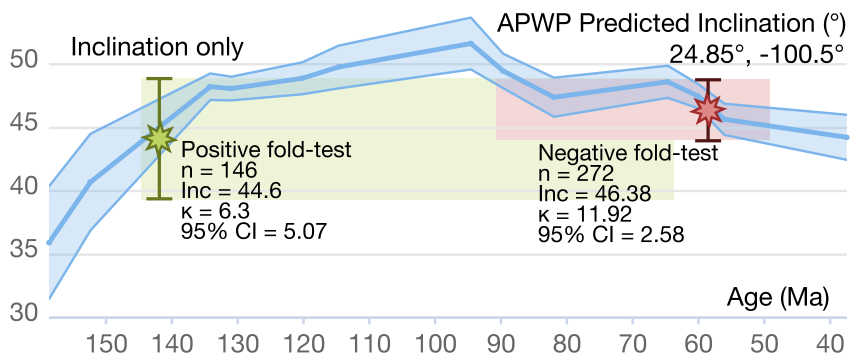


**Figure 9.** Global Apparent Polar Wander Path (GAPWaP of Vaes et al., 2023) showing average inclination of pre-folding localities and the syn- and post-folding with inclination-only statistics (Arason & Levi, 2010). The results show average inclination (Inc) of all pre-folding inclinations  $44.6^\circ \pm 5.07^\circ$  and  $46.4^\circ \pm 2.58^\circ$  for syn- and post-folding.  $n$ , number of samples;  $k$ , concentration parameter and 95% CI: confidence interval at 95% confidence.

Geologists typically assume that during vertical-axis rotations, the orogenic trend and the geological fabric rotate together, maintaining a constant angle between them along the curvature of the orogen. However, users of the orocline test should be aware that certain fabrics may develop with a curved geometry due to strain–stress refraction effects caused by local or regional anisotropies, such as lateral facies variations or contrasting rheologies of adjacent crustal blocks (e.g., Yonkee & Weil, 2010). In contrast, paleomagnetic directions are independent of structural evolution or paleogeographic context and, if properly constrained for the timing of magnetization acquisition, provide unequivocal evidence of vertical-axis rotations.

The slope ( $m$ ) of a regression between strike and fabric indicates the proportion of orogenic curvature acquired after the formation of the given fabric, assuming that it was originally parallel (to the stress field, the magnetic field, etc.). The resulting slope from the orocline test can be interpreted in terms of two end-members (slopes 0 and 1) and an intermediate case. If orogenic curvature is not due to vertical-axis rotations, we call it a primary feature. In contrast, secondary oroclines (where the fabric formed before vertical-axis rotations and rotated with the orocline limbs) will show a slope of 1, meaning 100% of the curvature developed after the fabric. In cases where the fabric or magnetization was acquired during rotation, or where part of the curvature is primary and was later tightened, the orocline test will yield a slope between 0 and 1, depending on the amount of pre-existing curvature at the time of fabric formation.

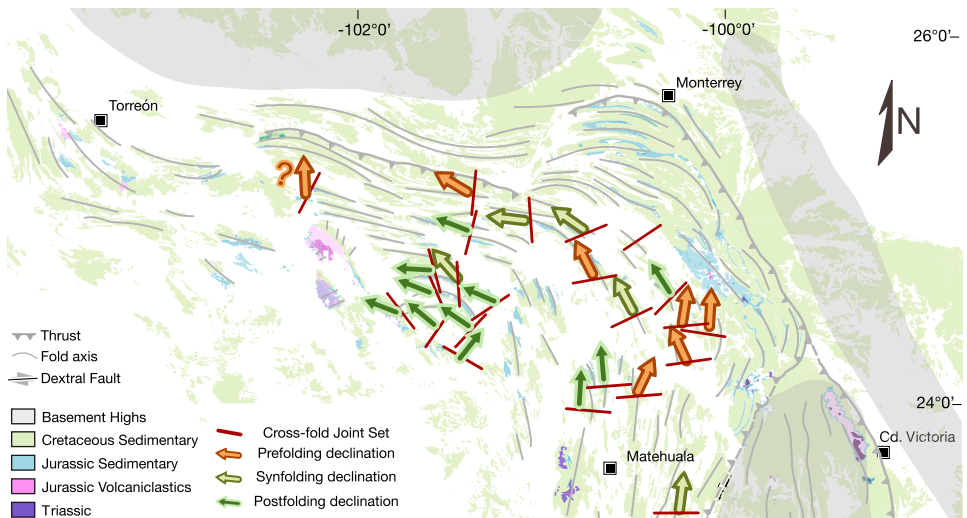


**Figure 10.** Geological map showing declinations in their best-fit coordinates of each fold test (i.e., geographic, tilt corrected, or with a given percentage of unfolding, cf. Table 1), and average cross-fold joints orientations. White represents Quaternary cover.

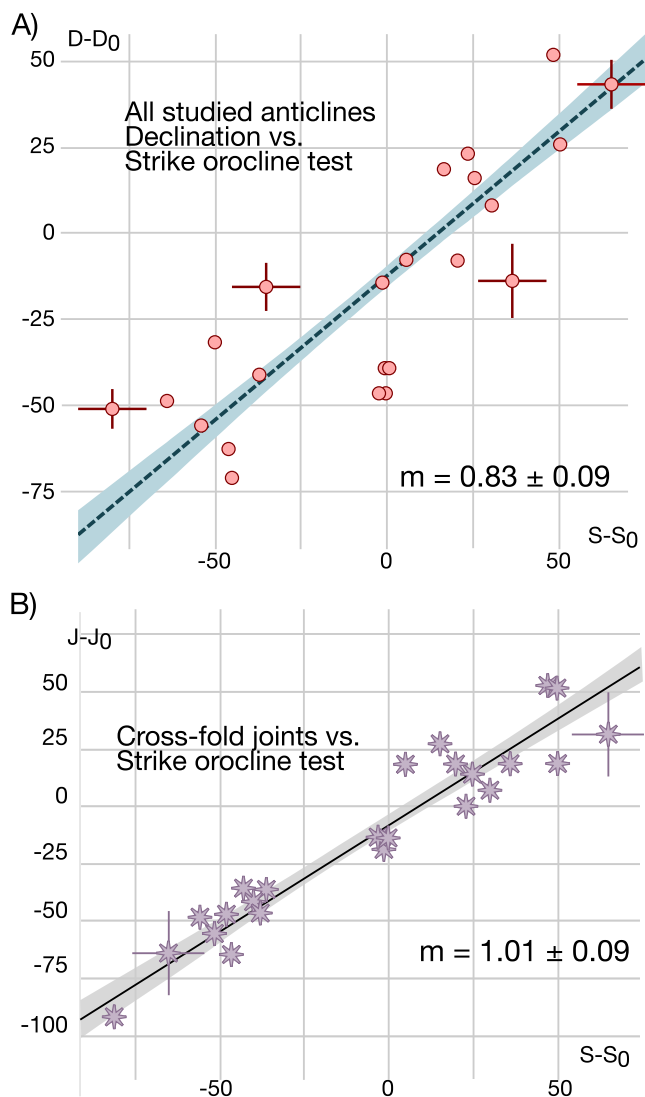


**Figure 11.** Bootstrapped orocline test (Pastor-Galán et al., 2017) of all the studied anticlines. (a) Paleomagnetic declinations versus structure strike. Uncertainties at a 95% confidence level have been removed for clarity and can be found in the raw data sets; two uncertainties are given per test as an example of their typical magnitudes. (b) Cross-fold joints versus structure strike. Paleomagnetic declinations show a slope of  $0.83 \pm 0.09$ , and the slope for cross-fold joints is  $1.01 \pm 0.09$ . Those results imply that the fold-and-thrust belt was originally linear and bent around a vertical axis subsequently.

the criteria established by Deenen et al. (2011) for sediment localities (at least  $n = 7$  and  $A95\text{min} \leq A95 \leq A95\text{max}$ ), indicating that the sampled localities are good recorders of the geomagnetic field. We discarded locality SRM2 due to its low number of valid data points (4) and large scatter, which did not permit a meaningful fold test. We retained the other localities (LG1, PLC2, SJC1, SJR1) despite their high concentration parameter ( $k > 50$ ), as they still show acceptable statistical parameters for sedimentary rocks when combined with the other fold limb at the respective location (see Table S2 in Supporting Information S1).

The fold-tests showed pre-, post-, and syn-folding best fits. Although syn-folding remanence could be attributed to acquisition during folding, Tauxe and Watson (1994) demonstrated that this behavior might also result from vertical axis rotation. Therefore, the origin of that remanence may not be syn-folding but rather an artifact of structural complications, such as one limb rotating around a vertical axis more than the other. The four cases that exhibit syn-folding remagnetization are better concentrated below 50% unfolding (Figure 7, Table 2). Thus, we

If the Sierra Madre Oriental were a primary feature, such as an inherited physiographic embayment, no curvature would have developed after the formation of parallel fabrics. In that case, regardless of the timing of magnetization, the slope of the orocline tests would be approximately zero (Pastor-Galán et al., 2011, 2017; Sussman & Weil, 2004; Yonkee & Weil, 2010). In contrast, if orocline tests on parallel fabrics that formed before or during the formation of a rectilinear thin-skinned fold-and-thrust belt yield a slope of one, this would show that vertical-axis rotations took place entirely after the belt was established. Finally, if the Sierra Madre Oriental bent synchronously with the development of the Sevier-style fold-and-thrust belt, the orocline tests should yield progressively decreasing slopes, reflecting the amount of curvature already in place at the time each fabric developed. We used the Bootstrapped Total Least Squares Orocline Test (Pastor-Galán et al., 2017) to evaluate the curvature of the Sierra Madre Oriental Orocline with respect to paleomagnetic declinations and strike-perpendicular joint sets. This method incorporates measurement uncertainty in paleomagnetic analyses ( $\Delta\text{Dec}$ ) and an estimated uncertainty for joint analysis layer parallel shortening directions (typically  $\pm 10^\circ$ ; Pastor-Galán et al., 2011). We estimated the anticlines' structural trend from the fold axis trend and local bedding strike, with a typical uncertainty of  $10^\circ$ . At least 25 localities are required to perform an accurate orocline test in a  $110^\circ$  curvature as the Sierra Madre Oriental Orocline (Pastor-Galán et al., 2017). However, we performed seven tests on various subsets of our data to evaluate potential differences in vertical axis rotation depending on the magnetization timings. Some of the tests have as little as 4 localities, so their confidence interval might be too large to be quantitative. These tests are as follows: (a) four tests considering paleomagnetic declinations separately based on their magnetization timing relative to folding (two pre-folding tests, one including NSJ and other without it, one syn-folding test, and one post-folding test); (b) one test considering all declinations together (Figure 11a); (c) one test considering all declinations together, including those of Guerra Roel et al. (2024); and (d) one test comparing the strike of the orogen with the cross-fold joint set (Figure 11b). The slope results of the tests (summarized in Table 2) range from 0.59 (pre-folding including NSJ) to 1.01 (cross-fold joints). The confidence intervals for all orocline tests overlap except for the pre-folding test with NSJ, where the outlier critically affects the result (0.59 with NSJ, 0.84 without it).

## 4. The Sierra Madre Oriental: Gone Around the Bend

### 4.1. Paleomagnetic Directions

Of the 671 sampled cores, 90.6% yielded interpretable ChRM directions, and only 2.1% of the valid directions required great circle fitting using other samples' ChRM as set points. Most of the localities (45 out of 50, or 90%) met

**Table 2**  
*Summary of the Orocline Tests*

Orocline tests	n	Total least squares	Average bootstrap	Confidence interval
Prefolding (with NSJ)	7	0.59	0.59	0.44–0.76
Prefolding <sup>a</sup>	6	0.83	0.84	0.68–1.03
Synfolding <sup>a</sup>	4	0.77	0.77	0.61–0.96
Postfolding <sup>a</sup>	12	0.89	0.89	0.77–1.03
All <sup>a</sup>	22	0.83	0.83	0.75–0.92
All and literature <sup>a</sup>	30	0.89	0.89	0.83–0.95
Cross-fold joints	25	1.01	1.01	0.92–1.10

<sup>a</sup>NSJ excluded from the analysis.

interpret that their NRM was acquired either syn-folding or post-folding, which means it occurred after 90 Ma, when folding began in the area (e.g., Fitz-Díaz et al., 2018).

After the structural correction that allows for the best concentration of the paleomagnetic directions, the declinations of the localities notably vary from ~W to ~NE (Figure 10; Table 1), which essentially conforms to the strike of the fold axis at the respective locality. This is consistent with vertical axis rotations due to orocline bending/buckling (Guerra Roel et al., 2024). Only NSJ1 and NSJ2 do not follow this curved trend. Inclinations are always downwards with one exception (NSJ1; Table S2 in Supporting Information S1). The anticline NSJ represents an outlier both in declination behavior with respect to the orogen strike and in its dual-polarity ChRM. The field data or laboratory results were in line with all other localities. NSJ2 shows the expected rotation in geographic coordinates, assuming that all NSJ declinations would follow the same pattern as the rest. However, NSJ1 shows a direction not found in any of the studied sites, regardless of the strike orientation. NSJ1 is one of the few localities where we identified a second component (mid-temperature and mid-coercivity) in most of the analyzed specimens (Table S1 in Supporting Information S1). We speculate that the NSJ1 ChRM component might not have been properly resolved due to partial remagnetization, resulting in a mixture of both components.

We find the observation of a single polarity along the belt somewhat surprising. The possibility of a common remagnetization event for the entire Taraises Formation during the Cretaceous Normal Superchron (e.g., Yoshimura, 2022) is difficult to reconcile with the other available constraints. The time window to acquire both pre- and post-folding magnetizations is limited to the deformation ages, ranging between 90 and 65 Ma. Given that the Cretaceous superchron ended at 84 Ma (Yoshimura, 2022), the remagnetization interpretation would be restricted to a narrow time interval. If remagnetization occurred throughout the Taraises Formation within this window, it would require a specific event capable of producing it, while at the same time affecting the Taraises only and not other adjacent units that seem to be remagnetized at different times (see Guerra Roel et al., 2024). We find this difficult to explain. In contrast, the dispersion of pre-folding magnetizations matches well with expectations for a primary detrital remanent magnetization, despite not showing reversals.

To constrain the timing of the magnetization acquisition, we have calculated a grand mean inclination for the anticlines showing pre-folding magnetizations and those depicting syn- and post-folding characteristics. The inclination of the former ( $44.6^\circ \pm 5^\circ$ ) fits well with the time of formation of the Taraises Formation (145–130 Ma) but not with any time younger than its formation (130 Ma) and the beginning of folding in the area (90 Ma; Figure 9). In the case of the syn- and post-folding anticlines, the inclination fits well with any time between the beginning of folding in the area (~90 Ma) and the end of the Mexican orogen (~40 Ma; Figure 9). Thus, we tentatively interpret that the Taraises Formation retains a primary NRM in some cases but was remagnetized in many other cases, either during or after folding associated with the “Sevier” event (Late Cretaceous). Within the studied Taraises Formation, post-folding remagnetization is more common in the core of the orocline, whereas pre-folding magnetization is more frequent in its outer arc (Figure 10). We did not observe any significant differences in the magnetic properties among the three identified magnetization components. The simplest explanation may be the proximity to the hinterland (located to the west). However, previous studies (e.g., Guerra Roel et al., 2024; Nemkin et al., 2019) have reported multiple remagnetization events, including post-folding remagnetization, in areas as far from the hinterland as the Monterrey Salient and to the north of Ciudad

Victoria (Figure 1; Guerra Roel et al., 2024). Additional paleomagnetic and, in particular, rock magnetic analyses are needed to better constrain the timing and mechanisms driving remagnetization in the Sierra Madre Oriental.

#### 4.2. Joint Analysis

We identified a systematic joint set in the 25 sampled anticlines along the trace of the Sierra Madre Oriental Orocline (Figure 10; Figure S2 in Supporting Information S1). This joint set, roughly perpendicular to the fold axis trend, corresponds to the classical cross-fold joint set described in many fold-and-thrust belts (e.g., Engelder & Geiser, 1980; Pastor-Galán et al., 2011). The joints exhibit a fan-like pattern with orientations diverging from north to southeast. Given the significant correlation between joint orientation and the arcuate trace of the Sierra Madre Oriental, it is challenging to envision a regional stress field that could have formed curved fold axes and in situ joint sets with a primary dispersion of 110°. Considering that the previous paleomagnetic analysis (Guerra Roel et al., 2024, and references therein) and the results presented in this paper (Section 4.1) support significant vertical axis rotations, it is more plausible that the joint set initially formed under a regional compression field with a roughly east-west trend that was subsequently rotated to its current orientation.

#### 4.3. The Twisted Kinematics of the Sierra Madre Oriental

The orocline test is an effective tool for studying the kinematics of curved mountain belts (e.g., Meijers et al., 2015; Yonkee & Weil, 2010). In this study, we combined paleomagnetic data and joint analysis to determine the kinematics of the Sierra Madre Orocline formation, which is currently poorly constrained (ranging from 120 Ma to 50 Ma, following Guerra Roel et al., 2024). Our paleomagnetic analysis identified three groups of anticlines based on the timing of their magnetization: (a) pre-folding, with likely primary magnetization acquired around 140 Ma; (b) syn-folding, with magnetization acquired after 90 Ma; and (c) post-folding, with magnetization younger than approximately 66 Ma. Additionally, joint sets likely develop very early in the deformation process (e.g., Engelder & Geiser, 1980), so we can consider the joint set orocline test as faithfully representing conditions ca. 90 Ma.

All but one of the orocline tests (Table 2) support a nearly 1:1 correlation between the strike and the studied fabrics (paleomagnetic declinations and cross-fold joint sets). Ironically, the exception is the pre-folding magnetization (~140 Ma), which shows the smallest slope ( $m = 0.59$ ). This result indicates that 60% of the rotation occurred from 140 Ma onwards. In contrast, post-folding magnetizations yield a slope of 0.89, suggesting that ~90% of the orocline formation happened after 66 Ma. This apparent contradiction disappears when we discard the outlying declination of the NSJ anticline from the orocline test (see Section 4.1). Once removed, the slopes of the pre-folding (0.84 95% CI [0.68–1.03]), joint sets (1.01 95% CI [0.92–1.10]), syn-folding (0.77 95% CI [0.61–0.96]), and post-folding (0.89 95% CI [0.77–1.03]) orocline tests are within confidence intervals (Table 2). The small differences can be attributed to the limited number of data points (~25) for the 110° curvature in the Sierra Madre Oriental (see Pastor-Galán et al., 2017).

Due to the similarities between the individual strike versus declination orocline tests, we can confidently perform a test with all paleomagnetic data but NSJ from this study ( $n = 22$ ). Combining all results allows us to get a more accurate and precise orocline formation kinematics estimation from paleomagnetism (Figure 11; Table 2; Pastor-Galán et al., 2017). This orocline test has a slope  $m = 0.83 \pm 0.09$  (Table 2). An orocline test with the studied anticlines in the Taraises Formation and the data included in Guerra Roel et al. (2024) yields  $m = 0.89 \pm 0.06$ . These two orocline tests, together with the joint sets ( $1.01 \pm 0.09$ ) establish that the Sierra Madre Oriental was originally an approximately linear fold-and-thrust belt that subsequently bent or buckled to form the Sierra Madre Oriental Orocline.

The simplest kinematic scenario that integrates structural and geochronological data and explains our new observations is synthesized in Figure 12. We hypothesize that the Mexican Fold and Thrust belt during the Late Cretaceous was an approximately linear belt with a nearly N-S strike of its fold axes and E-W oriented cross-fold joints (present-day coordinates). During and shortly after the deformation, part of the Taraises Formation was remagnetized. Sometime after the remagnetization, the whole belt underwent vertical axis rotations. The northern limb of the orocline accommodated up to 90° of counterclockwise rotation, whereas the southern limb accommodated <30° clockwise rotation, both with respect to the Maastrichtian-Eocene segment of the GAPWaP rotated to North American coordinates, Vaes et al. (2023), Guerra Roel et al. (2024). Whether and how the basement highs were involved in the rotations cannot be assessed with the available kinematic data. During the orocline

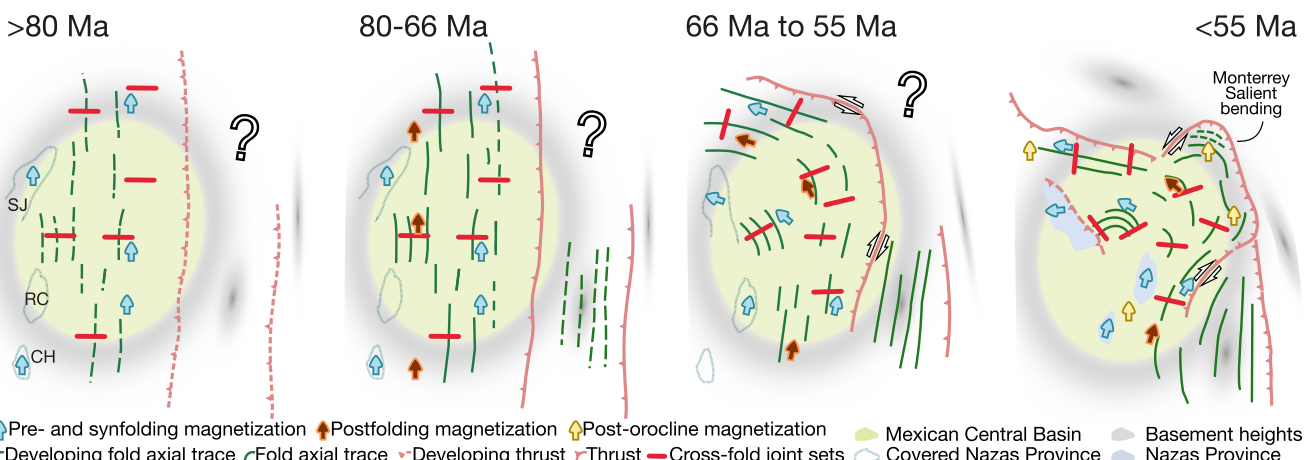


**Figure 12.** Cartoon showing the proposed kinematic evolution of the Sierra Madre Oriental Orocline, where the main structures of the fold-and-thrust belt formed prior to the orocline bending process. Arrows illustrate a simplified interpretation of the magnetization components identified in this study and those described by Guerra Roel et al. (2024). Dashed lines represent developing structures, pale-green shading: general distribution of the Mexican Central Basin. Light blue outlines and shaded areas correspond to outcrops of the Nazas Province with significant vertical axis rotations studied by Guerra Roel et al. (2024). SJ, San Julian Uplift; RC, Real de Catorce area; CH, Charcas area.

bending/buckling process, and likely due to the space problems generated by the rotation of the hinge, the Monterrey Salient began folding at ~60–50 Ma (Nemkin et al., 2019). Finally, after the orocline formation was completed, the Laramide-style thick-skinned tectonic event occurred, cross-cutting the curved shape of the orocline (e.g., see the Norias fault in the San Julián block; Figure 1). If the basement highs rotated during the process, it would imply a mechanism capable of bending the entire lithosphere, including rigid blocks. However, their involvement might have been passive: the basement highs may not have rotated themselves, but instead forced the belt to accommodate a pre-existing angular geometry. This kinematic scenario calls for a geodynamic mechanism. We cannot confidently identify one, but we consider it useful to hypothesize on possible formation mechanisms.

Considering that no evidence of superimposed folds or other structures indicating major changes in the stress field has been reported so far (see Weil et al. (2013) for the expected structures formed during orocline buckling), we are inclined to favor bending over buckling as the formation mechanism. The subduction of the Farallon and Pacific plates below the North American plate is the main geodynamic process that could play a significant role in the orocline bending process. The Cocos slab and the imaged Farallon subducted plate contain steep thickened segments and low-angle “flat slab” segments in the upper mantle and in the upper lower mantle (Boschman et al., 2018). The observed variations in the geometry of the slab suggest episodes of trench retreat and advance, which these subduction scenarios translate to extension and shortening events, respectively (Heuret & Lallemand, 2005; Lallemand et al., 2005). These episodes have been proposed to explain the formation and subsequent closure of Mesozoic basins, including the Mexican Central Basin (Fitz-Díaz et al., 2018). One rather preliminary option suggests that an irregular coastline, defined by basement highs, promoted differential extension during the opening of the Arperos back-arc basin. The subsequent closure of the basin would have led to continued shortening in the Mexican Central Basin (Fitz-Díaz et al., 2018), initially producing approximately rectilinear folding and eventually resulting in vertical-axis rotations and deformation in the Monterrey Salient. This model can explain the observed consistency in cross-fold joint-set orientation without the development of additional joint sets. Finding additional joint sets would imply evolving stress fields as found in buckling oroclines (e.g., Pastor-Galán et al., 2011, 2014; Whitaker & Engelder, 2006). In contrast, this proposed model would require significantly larger along-strike variations in shortening in the foreland fold-and-thrust belt than those reported (Fitz-Díaz et al., 2018).

A second option is that subduction of features such as oceanic plateaus, seamounts, or immature island arcs is a mechanism that can induce orogen bending (e.g., Betts et al., 2015). This type of orocline bending has been suggested in the Kanto syntaxis in Japan (Hoshi & Sano, 2013) and in the Central Asian Orogenic Belt (Yang, 2020). We speculate that the subduction of the Hess, or a similar oceanic plateau, beneath northern Mexico

during the Maastrichtian to Early Eocene (Liu et al., 2010) could represent a potential mechanism for generating the differential deformation required to bend the Sierra Madre Oriental. This process may account for both the development of the Monterrey salient and the possible involvement and bending of basement highs, should they have participated in the orocline formation. Additionally, plateau subduction is thought to produce flat subduction (Fitz-Diaz et al., 2018), which could account for the distribution pattern of magmatic rocks in the Sierra Madre Oriental. A weak aspect of this model is the absence of fragments of the plateau or accreted seamounts to the west of the Guerrero arc.

An alternative solution involving subduction zone dynamics may be related to along-strike changes in the subduction velocities and/or slopes as suggested for the formation of the Bolivian Orocline (e.g., Capitanio et al., 2011) or the Olympic orocline in Cascadia (Finley et al., 2019). A model like this would involve two main structural processes to accommodate bending of the Sierra Madre Oriental: strike-slip or flexural slip along the orocline limbs, structures apparently present in some areas (Figure 10); and localized shortening in the core of the fold, particularly evident in the Monterrey salient (Figures 10 and 12). In this scenario, oroclinal bending is promoted and maintained by along-strike variations in the subduction zone, likely controlled by changes in subduction geometry at depth. This mechanism could explain the concave-outboard margin and the structural architecture, although it seems less effective in accounting for the magmatic rock distribution in the region.

Our research presents in detail kinematic constraints for the formation of a secondary orocline in the Sierra Madre Oriental. Understanding the origin of the Sierra Madre Oriental Orocline is a crucial step toward deciphering the broader tectonic evolution of Pacific tectonics. However, the tectonic and geodynamic mechanisms behind the formation of this orocline are unknown and unexplored. The models we outline here only represent starting hypotheses intended to stimulate further investigation and scientific discussion. We anticipate that future research integrating structural, geophysical, geochronological, and petrological data will refine, challenge, or expand upon these ideas.

## 5. Conclusions

The Taraises Formation in the Sierra Madre Oriental fold-and-thrust belt shows pre-, syn-, and post-folding magnetizations. We propose a (pseudo-)primary origin for the pre-folding magnetizations, whereas the syn- and post-folding magnetizations likely reflect remagnetizations associated with the thin-skinned Sevier event (110–50 Ma). Our results reveal large-scale counterclockwise vertical-axis rotations (~90°) in the northern limb of the orocline and moderate clockwise rotations (<30°) in the southern limb. The Sierra Madre Oriental developed as a rectilinear fold-and-thrust belt with a roughly N–S strike parallel to the subduction trench. Its present curvature resulted from orocline bending between 66 and 55 Ma.

## Conflict of Interest

The authors declare no conflicts of interest relevant to this study.

## Data Availability Statement

The paleomagnetic and rock magnetic data used in the study are available at ZENODO via Pastor-Galán (2025) (<https://doi.org/10.5281/zenodo.14742739>), with a Creative Commons Attribution 4.0 International license Data can be found in <https://doi.org/10.5281/zenodo.14742739>. Paleomagnetic data can be also found in the [paleomagnetism.org](https://paleomagnetism.org) database in the following link <https://paleomagnetism.org/publication/?f0287d4f97a4150e40418ac7a4275b2d70e95b501c2428018d66686355c128ad>.

## References

- T. H. Anderson, J. A. Nourse, J. W. McKee, & M. B. Steiner (Eds.) (2005). *The Mojave-Sonora megashear hypothesis: Development, assessment, and alternatives* (Vol. 393, pp. 1–50). Geological Society of America.
- Arason, P., & Levi, S. (2010). Maximum likelihood solution for inclination-only data in paleomagnetism. *Geophysical Journal International*, 182(2), 753–771. <https://doi.org/10.1111/j.1365-246X.2010.04671.x>
- Betts, P. G., Moresi, L., Miller, M. S., & Willis, D. (2015). Geodynamics of oceanic plateau and plume head accretion and their role in Phanerozoic orogenic systems of China. *Geoscience Frontiers*, 6(1), 49–59. <https://doi.org/10.1016/j.gsf.2014.07.002>
- Blauser, W. H., & McNulty, C. L. (1981). Calpionellids and Nannoconids of Taraises Formation (Early Cretaceous), Santa Rosa Canyon, Sierra de Santa Rosa, Nuevo Leon, Mexico. *AAPG Bulletin*, 64(9), 1554.

## Acknowledgments

We thank the reviewers Elena Zanella, Claudio Robustelli Test, Arlo Weil and Adolph Yonkee for their thorough and constructive reviews, which have helped us make this study much better. RGR thanks the CONACYT for the support in the form of a doctoral scholarship, for support by a Ramón y Cajal Fellow Grant awarded to DPG (RYC2019-028244-I) funded by MCIN/AEI/10.13039/501100011033, and for support by the “European Social Fund Investing in your future.” DPG is funded by Grant PID2021-128801NA-I00 funded by MCIN/AEI/10.13039/501100011033, a Ramón y Cajal Fellow Grant RYC2019-028244-I funded by MCIN/AEI/10.13039/501100011033, and by the “European Social Fund Investing in your future”, and a Leonardo Grant 2022 to researchers and cultural creators (LEO22-2-3010) from the BBVA bank. GCC is grateful for the support from PAICYT projects: CT12 48-20, CT1626-21, and 36-CAT-2022. JJAG gratefully acknowledges PAPIIT UNAM Grants IN106820 and IG101523. This paper is dedicated to the loving memory of Roberto Stanley Molina Garza, whose brutal, unsolved murder demands justice.

- Borradaile, G. J., & Jackson, M. (2010). Structural geology, petrofabrics and magnetic fabrics (AMS, AARM, AIRM). *Journal of Structural Geology*, 32(10), 1519–1551. <https://doi.org/10.1016/j.jsg.2009.09.006>
- Boschman, L. M., van Hinsbergen, D. J. J., Kimbrough, D. L., Langereis, C. G., & Spakman, W. (2018). The dynamic history of 220 million years of subduction below Mexico: A correlation between slab geometry and overriding plate deformation based on geology, paleomagnetism, and seismic tomography. *Geochemistry, Geophysics, Geosystems*, 19(12), 4649–4672. <https://doi.org/10.1029/2018GC007739>
- Busby, C. J., & Centeno-García, E. (2022). The “Nazas Arc” is a continental rift province: Implications for Mesozoic tectonic reconstructions of the southwest Cordillera, US and Mexico. *Geosphere*, 18(2), 647–669. <https://doi.org/10.1130/ges02443.1>
- Busby, C. J., Whitmeyer, S. J., Williams, M. L., Kellett, D. A., & Tikoff, B. (2023). *Guerrero-Alisitos-Vizcaino superterrane of western Mexico and its ties to the Mexican continental margin (Gondwana and SW Laurentia). In Laurentia: Turning points in the evolution of a continent* (Vol. 220, p. 0). Geological Society of America. [https://doi.org/10.1130/2022.1220\(34\)](https://doi.org/10.1130/2022.1220(34))
- Centeno-García, E., Guerrero-Suastegui, M., & Talavera-Mendoza, O. (2008). The Guerrero composite terrane of western Mexico: Collision and subsequent rifting in a supra-subduction zone. In A. E. Draut, P. D. Clift, & D. W. Scholl (Eds.), *Formation and applications of the sedimentary record in arc collision zones* (Vol. 436, p. 0). Geological Society of America. [https://doi.org/10.1130/2008.2436\(13\)](https://doi.org/10.1130/2008.2436(13))
- Campa, M. F., & Conej, P. J. (1983). Tectono-stratigraphic terranes and mineral resource distributions in Mexico. *Canadian Journal of Earth Sciences*, 20(6), 1040–1051. <https://doi.org/10.1139/e83-094>
- Capitanio, F. A., Faccenna, C., Zlotnik, S., & Stegman, D. R. (2011). Subduction dynamics and the origin of Andean orogeny and the Bolivian orocline. *Nature*, 480(7375), 83–86. <https://doi.org/10.1038/nature10596>
- Carruthers, T., Moerland, M. S., Ebersbach, J., Favre, A., Folk, R. A., Hawkins, J. A., et al. (2024). Repeated upslope biome shifts in Saxifraga during late-Cenozoic climate cooling. *Nature Communications*, 15(1), 1100. <https://doi.org/10.1038/s41467-024-45289-w>
- Centeno-García, E. (2017). Mesozoic tectono-magmatic evolution of Mexico: An overview. *Ore Geology Reviews*, 81, 1035–1052. <https://doi.org/10.1016/j.oregeorev.2016.10.010>
- Chávez-Cabello, G., Aranda-Gómez, J. J., Molina-Garza, R. S., Cossío-Torres, T., Arvizu-Gutiérrez, I. R., & González-Naranjo, G. A. (2005). La falla San Marcos: Una estructura jurásica de basamento multirreactivada del noreste de México. *Boletín de La Sociedad Geológica Mexicana*, 57(1), 27–52.
- Chen, Y. W., Wu, J., Bunge, H. P., Stotz, I., Robl, G., & Schuberth, B. S. (2025). Tomopac2: An unfolded-slab plate reconstruction validated via mantle circulation models in a closed-loop experiment. *Proceedings of the royal society A* (Vol. 481(2318), p. 20240726). <https://doi.org/10.1098/rspa.2024.0726>
- DeCelles, P. G. (2004). Late Jurassic to Eocene evolution of the Cordilleran thrust belt and foreland basin system, western U.S.A. *American Journal of Science*, 304(2), 105–168. <https://doi.org/10.2475/ajs.304.2.105>
- DeCelles, P. G., & Graham, S. A. (2015). Cyclical processes in the north American Cordilleran orogenic system. *Geology*, 43(6), 499–502. <https://doi.org/10.1130/g36482.1>
- Deenen, M. H., Langereis, C. G., van Hinsbergen, D. J., & Biggin, A. J. (2011). Geomagnetic secular variation and the statistics of palaeomagnetic directions. *Geophysical Journal International*, 186(2), 509–520. <https://doi.org/10.1111/j.1365-246x.2011.05050.x>
- Dickinson, W. R. (2004). Evolution of the north American cordillera. *Annual Review of Earth and Planetary Sciences*, 32(32), 13–45. <https://doi.org/10.1146/annurev.earth.32.101802.120257>
- Dickinson, W. R., & Lawton, T. F. (2001). Carboniferous to Cretaceous assembly and fragmentation of Mexico. *Geological Society of America Bulletin*, 113(9), 1142–1160. [https://doi.org/10.1130/0016-7606\(2001\)113<1142:ctaaf>2.0.co;2](https://doi.org/10.1130/0016-7606(2001)113<1142:ctaaf>2.0.co;2)
- Domeier, M., & Torsvik, T. H. (2014). Plate tectonics in the late Paleozoic. *Geoscience Frontiers*, 5(3), 303–350. <https://doi.org/10.1016/j.gsf.2014.01.002>
- Eguiluz, S., Aranda, M., & Marrett, R. (2000). Tectónica de la Sierra Madre Oriental, México. *Boletín de La Sociedad Geológica Mexicana*, 53(1), 1–26.
- Eldredge, S., Bachtadse, V., & Van der Voo, R. (1985). Paleomagnetism and the orocline hypothesis. *Tectonophysics*, 119(1–4), 153–179. [https://doi.org/10.1016/0040-1951\(85\)90037-x](https://doi.org/10.1016/0040-1951(85)90037-x)
- Engebretson, D. C., Cox, A., & Gordon, R. G. (1985). Relative motions between oceanic and continental plates in the Pacific basin. In D. C. Engebretson, A. Cox, & R. G. Gordon (Eds.), *Relative motions between oceanic and continental plates in the Pacific basin* (Vol. 206, pp. 0–60). Geological Society of America. <https://doi.org/10.1130/SPE206-p1>
- Engelder, T., & Geiser, P. (1980). On the use of regional joint sets as trajectories of paleostress fields during the development of the Appalachian Plateau, New York. *Journal of Geophysical Research*, 85(B11), 6319–6341. <https://doi.org/10.1029/JB085iB11p06319>
- Finley, T., Morell, K., Leonard, L., Regalla, C., Johnston, S. T., & Zhang, W. (2019). Ongoing oroclinal bending in the Cascadia forearc and its relation to concave-outboard plate margin geometry. *Geology*, 47(2), 155–158. <https://doi.org/10.1130/45473.1>
- Fitz-Díaz, E., Hall, C. M., & van der Pluijm, B. A. (2016). XRD-Based 40Ar/39Ar age correction for fine-grained Illite, with application to folded carbonates in the Monterrey Salient (northern Mexico). *Geochimica et Cosmochimica Acta*, 181, 201–216. <https://doi.org/10.1016/j.gca.2016.02.004>
- Fitz-Díaz, E., Hudleston, P., Tolson, G., & van der Pluijm, B. (2014). Progressive, episodic deformation in the Mexican fold-thrust belt (central Mexico): Evidence from isotopic dating of folds and faults. *International Geology Review*, 56(6), 734–755. <https://doi.org/10.1080/00206814.2014.896228>
- Fitz-Díaz, E., Lawton, T. F., Juárez-Arriaga, E., & Chávez-Cabello, G. (2018). The Cretaceous-Paleogene Mexican orogen: Structure, basin development, magmatism and tectonics. *Earth-Science Reviews*, 183, 56–84. <https://doi.org/10.1016/j.earscirev.2017.03.002>
- Fuston, S., & Wu, J. (2020). Raising the resurrection plate from an unfolded-slab plate tectonic reconstruction of northwestern north America since early Cenozoic time. *GSA Bulletin*, 133(5–6), 1128–1140. <https://doi.org/10.1130/B35677.1>
- Goldammer, R. K. (1999). Mesozoic sequence stratigraphy and paleogeographic evolution of northeast Mexico. *Mesozoic Sedimentary and Tectonic History of North-central Mexico*, 340, 1–58. <https://doi.org/10.1130/0-8137-2340-x.1>
- Goldammer, R. K., & Johnson, C. A. (2001). Middle Jurassic–upper Cretaceous paleogeographic evolution and sequence-stratigraphic framework of the northwest Gulf of Mexico rim. In C. Bartolini, R. T. Buffler, & A. Cantú-Chapé (Eds.), *The western Gulf of Mexico basin: Tectonics, sedimentary basins, and petroleum systems* (Vol. 75, p. 0). American Association of Petroleum Geologists. <https://doi.org/10.1306/m75768c3>
- Gross, M. R., Fischer, M. P., Engelder, T., & Greenfield, R. J. (1995). *Factors controlling joint spacing in interbedded sedimentary rocks: Integrating numerical models with field observations from the Monterrey formation*. Geological Society, London, Special Publications, (Vol. 92(1), pp. 215–233). <https://doi.org/10.1144/GSL.SP.1995.092.01.12>
- Guerra Roel, R. (2019). Análisis estructural de la zona Norte del bloque de San Julián, Zacatecas México [Masters, Universidad Autónoma de Nuevo León]. Retrieved from <http://eprints.uanl.mx/18367/>

- Guerra Roel, R., Pastor Galán, D., Chávez-Cabello, G., Ramírez-Peña, C. F., Aranda Gómez, J. J., Patiño Méndez, G., et al. (2024). The sierra Madre oriental Orocline: Paleomagnetism of the Nazas province in NE Mexico. *Journal of Geophysical Research: Solid Earth*, 129(9), e2024JB029239. <https://doi.org/10.1029/2024JB029239>
- Gutiérrez-Navarro, R., Fitz-Díaz, E., Barboza-Gudiño, J. R., & Stockli, D. F. (2021). Shortening and exhumation of Sierra de Catorce in northeastern Mexico, in light of 40Ar/39Ar Illite dating and (U-Th)/He zircon thermochronology. *Journal of South American Earth Sciences*, 111, 103334. <https://doi.org/10.1016/j.jsames.2021.103334>
- Hancock, P. L. (1985). Brittle microtectonics: Principles and practice. *Journal of Structural Geology*, 7(3), 437–457. [https://doi.org/10.1016/0191-8141\(85\)90048-3](https://doi.org/10.1016/0191-8141(85)90048-3)
- Heidbach, O., Reinecker, J., Tingay, M., Müller, B., Sperner, B., Fuchs, K., & Wenzel, F. (2007). Plate boundary forces are not enough: Second- and third-order stress patterns highlighted in the world stress map database. *Tectonics*, 26(6). <https://doi.org/10.1029/2007tc002133>
- Heuret, A., & Lallemand, S. (2005). Plate motions, slab dynamics and back-arc deformation. *Physics of the Earth and Planetary Interiors*, 149(1), 31–51. <https://doi.org/10.1016/j.pepi.2004.08.022>
- Hoshi, H., & Sano, M. (2013). Paleomagnetic constraints on Miocene rotation in the central Japan Arc. *Island Arc*, 22(2), 197–213. <https://doi.org/10.1111/iar.12022>
- Housen, B. A., & Beck Jr, M. E. (1999). Testing terrane transport: An inclusive approach to the Baja BC controversy. *Geology*, 27(12), 1143–1146. [https://doi.org/10.1130/0091-7613\(1999\)027<1143:tttaia>2.3.co;2](https://doi.org/10.1130/0091-7613(1999)027<1143:tttaia>2.3.co;2)
- Imlay, R. W. (1936). Evolution of the Coahuila peninsula, Mexico. Part IV. *Geology of the western part of the Sierra de Parras.*, 47(7), 1091–1152. <https://doi.org/10.1130/gsab-47-1091>
- Jelínek, V. (1977). *The statistical theory of measuring anisotropy of magnetic susceptibility of rocks and its application* (Vol. 29, pp. 1–87). Geofyzika.
- Johnston, S. T. (2001). The great Alaskan Terrane Wreck: Reconciliation of paleomagnetic and geological data in the northern Cordillera. *Earth and Planetary Science Letters*, 193(3), 259–272. [https://doi.org/10.1016/S0012-821X\(01\)00516-7](https://doi.org/10.1016/S0012-821X(01)00516-7)
- Juárez-Arriaga, E., Lawton, T. F., Solari, L. A., & Stockli, D. F. (2022). Stratigraphy and origin of upper Cretaceous wedge-top and proximal foredeep deposits in the Mexican foreland basin, east-central Mexico. *Journal of South American Earth Sciences*, 114, 103681. <https://doi.org/10.1016/j.jsames.2021.103681>
- Keppie, D. (2004). Terranes of Mexico revisited: A 1.3 billion year odyssey. *Internacional Geology Review*, 46(9), 765–794. <https://doi.org/10.2747/0020-6814.46.9.765>
- Keppie, J. D., & Ortega-Gutiérrez, F. (2010). 1.3–0.9 Ga oaxaquia (Mexico): Remnant of an arc/backarc on the northern margin of Amazonia. *Journal of South American Earth Sciences*, 29(1), 21–27. <https://doi.org/10.1016/j.jsames.2009.07.001>
- Kirschvink, J. (1980). The least-squares line and plane and the analysis of palaeomagnetic data. *Geophysical Journal International*, 62(3), 699–718. <https://doi.org/10.1111/j.1365-246x.1980.tb02601.x>
- Koymans, M. R., Langereis, C. G., Pastor-Galán, D., & van Hinsbergen, D. J. (2016). *Paleomagnetism.org: An online multi-platform open source environment for paleomagnetic data analysis*. Elsevier.
- Koymans, M. R., van Hinsbergen, D. J. J., Pastor-Galán, D., Vaes, B., & Langereis, C. G. (2020). Towards FAIR paleomagnetic data management through Paleomagnetism. Org 2.0. *Geochemistry, Geophysics, Geosystems*, 21(2), e2019GC008838. <https://doi.org/10.1029/2019gc008838>
- Lallemand, S., Heuret, A., & Boutelier, D. (2005). On the relationships between slab dip, back-arc stress, upper plate absolute motion, and crustal nature in subduction zones. *Geochemistry, Geophysics, Geosystems*, 6(9). <https://doi.org/10.1029/2005GC000917>
- Lawton, T. F. (1994). Tectonic setting of Mesozoic sedimentary basins, rocky Mountain region, United States. (pp. 1–26). [https://archives.datapages.com/data/rocky\\_sepm/data/032/032001/\\_rocky\\_mount320001.htm](https://archives.datapages.com/data/rocky_sepm/data/032/032001/_rocky_mount320001.htm)
- Liu, L., Gurnis, M., Seton, M., Saleeby, J., Müller, R. D., & Jackson, J. M. (2010). The role of oceanic plateau subduction in the Laramide orogeny. *Nature Geoscience*, 3(5), 353–357. <https://doi.org/10.1038/ngeo829>
- Maffione, M., Speranza, F., Cascella, A., Longhitano, S. G., & Chiarella, D. (2013). A~125 post-early Serravallian counterclockwise rotation of the gorgoglion formation (southern Apennines, Italy): New constraints for the formation of the Calabrian arc. *Tectonophysics*, 590, 24–37. <https://doi.org/10.1016/j.tecto.2013.01.005>
- Martini, M., Mori, L., Solari, L., & Centeno-García, E. (2011). Sandstone Provenance of the Arperos Basin (Sierra de Guanajuato, Central Mexico): Late Jurassic–early cretaceous back-arc spreading as the foundation of the Guerrero terrane. *The Journal of Geology*, 119(6), 597–617. <https://doi.org/10.1086/661989>
- Martini, M., & Ortega-Gutiérrez, F. (2018). Tectono-stratigraphic evolution of eastern Mexico during the break-up of Pangea: A review. *Earth-Science Reviews*, 183, 38–55. <https://doi.org/10.1016/j.earscirev.2016.06.013>
- Martini, M., Solari, L., & Camprubí, A. (2013). Kinematics of the Guerrero terrane accretion in the Sierra de Guanajuato, central Mexico: New insights for the structural evolution of arc–continent collisional zones. *International Geology Review*, 55(5), 574–589. <https://doi.org/10.1080/00206814.2012.729361>
- Martini, M., Solari, L., & López-Martínez, M. (2014). Correlating the Arperos basin from Guanajuato, central Mexico, to Santo Tomás, southern Mexico: Implications for the paleogeography and origin of the Guerrero terrane. *Geosphere*, 10(6), 1385–1401. <https://doi.org/10.1130/GES01055.1>
- McElhinny, M. W., & McFadden, P. L. (1999). *Paleomagnetism: Continents and Oceans*. Elsevier.
- McFadden, P. L., & McElhinny, M. W. (1988). The combined analysis of remagnetization circles and direct observations in palaeomagnetism. *Earth and Planetary Science Letters*, 87(1), 161–172. [https://doi.org/10.1016/0012-821X\(88\)90072-6](https://doi.org/10.1016/0012-821X(88)90072-6)
- Meijers, M., Smith, B., Pastor-Galán, D., Degenaar, R., Sadradze, N., Adamia, S., et al. (2015). *Progressive orocline formation in the Eastern Pontides-Lesser Caucasus*. Geological Society, London, Special Publications. <https://doi.org/10.1144/SP428.8>
- Michałzik, D. (1988). Trias bis tiefste Unter-Kreide der nordöstlichen Sierra Madre Oriental, Mexiko—Fazielle Entwicklung eines passiven Kontinentalrandes (pp. 1–247).
- Mullender, T. A., Frederichs, T., Hilgenfeldt, C., de Groot, L. V., Fabian, K., & Dekkers, M. J. (2016). Automated paleomagnetic and rock magnetic data acquisition with an in-line horizontal “2 g” system. *Geochemistry, Geophysics, Geosystems*, 17(9), 3546–3559. <https://doi.org/10.1002/2016gc006436>
- Mullender, T. a. T., van Velzen, A. J., & Dekkers, M. J. (1993). Continuous drift correction and separate identification of ferrimagnetic and paramagnetic contributions in thermomagnetic runs. *Geophysical Journal International*, 114(3), 663–672. <https://doi.org/10.1111/j.1365-246X.1993.tb06995.x>
- Müller, R. D., Zahirovic, S., Williams, S. E., Cannon, J., Seton, M., Bower, D. J., et al. (2019). A global plate model including lithospheric deformation along major rifts and orogens since the Triassic. *Tectonics*, 38(6), 1884–1907. <https://doi.org/10.1029/2018TC005462>
- Nemkin, S. R., Chávez-Cabello, G., Fitz-Díaz, E., van der Pluijm, B., & Van der Voo, R. (2019). Concurrency of folding and remagnetization events in the Monterrey Salient (NE Mexico). *Tectonophysics*, 760, 58–68. <https://doi.org/10.1016/j.tecto.2017.12.002>

- Nokleberg, W., Bundtzen, T. K., Eremin, R. A., Ratkin, V., Dawson, K. M., Shpkerman, V., et al. (2005). *Metallogenesis and tectonics of the Russian Far East, Alaska, and the Canadian Cordillera* (Vol. P1697, p. 397). USGS Professional Paper.
- Ocampo-Díaz, Y. Z. E., Pinzon-Sotelo, M. P., Chávez-Cabello, G., Ramírez-Díaz, A., Martínez-Paco, M., Velasco-Tapia, F., et al. (2016). Propuesta nomenclatural y Análisis de procedencia de la Formación Concepción del Oro (antes Formación Caracol): Implicaciones sobre la evolución tectónica del sur de Norteamérica Durante el Cretácico Tardío. *Revista Mexicana de Ciencias Geológicas*, 33(1), 3–33.
- Padilla y Sánchez, R. J. (1985). Las estructuras de la Curvatura de Monterrey, Estados de Coahuila, Nuevo León, Zacatecas y San Luis Potosí. *Revista Mexicana de Ciencias Geológicas*, 6(1), 1–20.
- Parés, J. M. (2015). Sixty years of anisotropy of magnetic susceptibility in deformed sedimentary rocks. *Frontiers in Earth Science*, 3. <https://doi.org/10.3389/feart.2015.00004>
- Parolari, M., Martini, M., Gómez-Tuena, A., Ortega-Gutiérrez, F., Errázuriz-Henao, C., & Cavazos-Tovar, J. G. (2022). The petrogenesis of Early–Middle Jurassic magmatism in southern and central Mexico and its role during the break-up of Western Pangaea. *Geological Magazine*, 159(6), 873–892. <https://doi.org/10.1017/s0016756822000061>
- Pastor-Galán, D. (2022). From supercontinent to superplate: Late Paleozoic Pangea's inner deformation suggests it was a short-lived superplate. *Earth-Science Reviews*, 226, 103918. <https://doi.org/10.1016/j.earscirev.2022.103918>
- Pastor-Galán, D. (2025). Bending the Sierra Madre Oriental: A Maastrichtian–Paleocene orocline (1.0) [Dataset]. Zenodo. <https://doi.org/10.5281/zenodo.14742739>
- Pastor-Galán, D., Gutiérrez-Alonso, G., & Weil, A. B. (2011). Orocline timing through joint analysis: Insights from the Ibero-Armorian Arc. *Tectonophysics*, 507(1), 31–46. <https://doi.org/10.1016/j.tecto.2011.05.005>
- Pastor-Galán, D., Martín-Merino, G., & Corrochano, D. (2014). Timing and structural evolution in the limb of an orocline: The Pisueña–Carrión Uní (southern limb of the Cantabrian Orocline, NW Spain). *Tectonophysics*, 622, 110–121. <https://doi.org/10.1016/j.tecto.2014.03.004>
- Pastor-Galán, D., Mulchrone, K. F., Koymans, M. R., van Hinsbergen, D. J. J., & Langereis, C. G. (2017). Bootstrapped total least squares orocline test: A robust method to quantify vertical-axis rotation patterns in orogens, with examples from the Cantabrian and Aegean oroclines. *Lithosphere*, 9(3), 499–511. <https://doi.org/10.1130/L547>
- Pfiffner, O. A. (2006). Thick-skinned and thin-skinned styles of continental contraction. In S. Mazzoli & R. W. H. Butler (Eds.), *Styles of Continental contraction* (p. 0). Geological Society of America. [https://doi.org/10.1130/2006.2414\(09](https://doi.org/10.1130/2006.2414(09)
- Pfiffner, O. A. (2017). Thick-Skinned and thin-skinned tectonics: A global perspective. *Geosciences*, 7(3), 71. <https://doi.org/10.3390/geosciences7030071>
- Ramírez-Peña, C. F., & Chávez-Cabello, G. (2017). Age and evolution of thin-skinned deformation in Zacatecas, Mexico: Sevier orogeny evidence in the Mexican Fold-Thrust Belt. *Journal of South American Earth Sciences*, 76, 101–114. <https://doi.org/10.1016/j.jsames.2017.01.007>
- Ramírez-Peña, C. F., Chávez-Cabello, G., Fitz-Díaz, E., Aranda-Gómez, J. J., & Valdés, R. S. (2019). Uplift and syn-orogenic magmatism in the Concepción del Oro Block: A thick-skinned (Laramide style?) contractional structure in the Mexican Fold-Thrust Belt. *Journal of South American Earth Sciences*, 93, 242–252. <https://doi.org/10.1016/j.jsames.2019.04.012>
- Scotese, C. R., Song, H., Mills, B. J. W., & van der Meer, D. G. (2021). Phanerozoic paleotemperatures: The earth's changing climate during the last 540 million years. *Earth-Science Reviews*, 215, 103503. <https://doi.org/10.1016/j.earscirev.2021.103503>
- Sedlock, R. L., Ortega-Gutiérrez, F., & Speed, R. C. (1993). *Tectonostratigraphic terranes and tectonic evolution of México* (Vol. 278, p. 153). Geological Society of America Special Paper.
- Sigloch, K., & Mihalynuk, M. G. (2013). Intra-oceanic subduction shaped the assembly of Cordilleran North America. *Nature*, 496(7443), 50–56. <https://doi.org/10.1038/nature12019>
- Sigloch, K., & Mihalynuk, M. G. (2017). Mantle and geological evidence for a late Jurassic–Cretaceous suture spanning North America. *GSA Bulletin*, 129(11–12), 1489–1520. <https://doi.org/10.1130/B31529.1>
- Sussman, A. J., & Weil, A. B. (2004). *Orogenic curvature: Integrating paleomagnetic and structural analyses*. Geological Society of America.
- Suter, M. (1984). Cordilleran deformation along the eastern edge of the Valles–San Luis Potosí carbonate platform, Sierra Madre oriental fold-thrust belt, east-central Mexico. *Geological Society of America Bulletin*, 95(12), 1387–1397. [https://doi.org/10.1130/0016-7606\(1984\)95<1387:cdate>2.0.co;2](https://doi.org/10.1130/0016-7606(1984)95<1387:cdate>2.0.co;2)
- Suter, M. (1990). *Hoja Tamazunchale 14Q-(5), con Geología de la Hoja Tamazunchale, Estados de Hidalgo, Querétaro y San Luis Potosí: Mexico City* (p. 56). Universidad Nacional Autónoma de México. Instituto de Geología, Carta Geológica de México, scale 1:100, 000.
- Tauxe, L., & Watson, G. S. (1994). The fold test: An Eigen analysis approach. *Earth and Planetary Science Letters*, 122(3), 331–341. [https://doi.org/10.1016/0012-821X\(94\)90006-X](https://doi.org/10.1016/0012-821X(94)90006-X)
- Torsvik, T. H., Steinberger, B., Shephard, G. E., Doubrovine, P. V., Gaina, C., Domeier, M., et al. (2019). Pacific–Panthalassic reconstructions: Overview, errata and the way forward. *Geochemistry, Geophysics, Geosystems*, 20(7), 3659–3689. <https://doi.org/10.1029/2019gc008402>
- Vaes, B., van Hinsbergen, D. J. J., van de Lagemaat, S. H. A., van der Wiel, E., Lom, N., Advokaat, E. L., et al. (2023). A global apparent polar wander path for the last 320 Ma calculated from site-level paleomagnetic data. *Earth-Science Reviews*, 245, 104547. <https://doi.org/10.1016/j.earscirev.2023.104547>
- van der Meer, D. G., Torsvik, T. H., Spakman, W., van Hinsbergen, D. J. J., & Amaru, M. L. (2012). Intra-Panthalassa Ocean subduction zones revealed by fossil arcs and mantle structure. *Nature Geoscience*, 5(3), 215–219. <https://doi.org/10.1038/ngeo1401>
- van Velzen, A. J., & Zijderveld, J. D. A. (1995). Effects of weathering on single-domain magnetite in early Pliocene marine marls. *Geophysical Journal International*, 121(1), 267–278. <https://doi.org/10.1111/j.1365-246X.1995.tb03526.x>
- Weil, A. B., Gutiérrez-Alonso, G., & Wicks, D. (2013). Investigating the kinematics of local thrust sheet rotation in the limb of an orocline: A paleomagnetic and structural analysis of the Esla tectonic unit, Cantabrian–Asturian Arc, NW Iberia. *International Journal of Earth Sciences*, 102(1), 43–60. <https://doi.org/10.1007/s00531-012-0790-3>
- Weil, A. B., & Yonkee, A. (2023). The laramide orogeny: Current understanding of the structural style, timing, and spatial distribution of the classic foreland thick-skinned tectonic system. In S. J. Whitmeyer, M. L. Williams, D. A. Kellett, & B. Tikoff (Eds.), *Laurentia: Turning points in the evolution of a continent* (p. 0). Geological Society of America. [https://doi.org/10.1130/2022.1220\(33](https://doi.org/10.1130/2022.1220(33)
- Weil, A. B., Yonkee, A., & Schultz, M. (2016). Tectonic evolution of a laramide transverse structural zone: Sweetwater Arch, south central Wyoming. *Tectonics*, 35(5), 1090–1120. <https://doi.org/10.1002/2016tc004122>
- Weil, A. B., Yonkee, A., & Sussman, A. (2010). Reconstructing the kinematic evolution of curved mountain belts: A paleomagnetic study of Triassic red beds from the Wyoming salient, Sevier thrust belt, USA. *Bulletin*, 122(1–2), 3–23. <https://doi.org/10.1130/b26483.1>
- Weil, A. B., & Yonkee, W. A. (2012). Layer-parallel shortening across the Sevier fold-thrust belt and Laramide foreland of Wyoming: Spatial and temporal evolution of a complex geodynamic system. *Earth and Planetary Science Letters*, 357–358, 405–420. <https://doi.org/10.1016/j.epsl.2012.09.021>
- Whitaker, A. E., & Engelder, T. (2005). Characterizing stress fields in the upper crust using joint orientation distributions. *Journal of Structural Geology*, 27(10), 1778–1787. <https://doi.org/10.1016/j.jsg.2005.05.016>

- Whitaker, A. E., & Engelder, T. (2006). Plate-scale stress fields driving the tectonic evolution of the central Ouachita salient, Oklahoma and Arkansas. *GSA Bulletin*, 118(5–6), 710–723. <https://doi.org/10.1130/B25780.1>
- Williams, S. A., Singleton, J. S., Prior, M. G., Mavor, S. P., Cross, G. E., & Stockli, D. F. (2021). The early Palaeogene transition from thin-skinned to thick-skinned shortening in the Potosí uplift, Sierra Madre oriental, northeastern Mexico. *International Geology Review*, 63(2), 233–263. <https://doi.org/10.1080/00206814.2020.1805802>
- Wright, N. M., Müller, R. D., Seton, M., & Williams, S. E. (2016). Revision of Paleogene plate motions in the Pacific and implications for the Hawaiian-emperor Bend: Reply. *Geology*, 44(4), e385. <https://doi.org/10.1130/g37828y.1>
- Yang, G. (2020). Kazakhstan Orocline bending in response to seamounts subduction. *Geological Journal*, 55(5), 3464–3475. <https://doi.org/10.1002/gj.3614>
- Yonkee, A., & Weil, A. B. (2010). Quantifying vertical axis rotation in curved orogens: Correlating multiple data sets with a refined weighted least squares strike test. *Tectonics*, 29(3), TC3012. <https://doi.org/10.1029/2008TC002312>
- Yonkee, W. A., & Weil, A. B. (2015). Tectonic evolution of the Sevier and Laramide belts within the North American Cordillera orogenic system. *Earth-Science Reviews*, 150, 531–593. <https://doi.org/10.1016/j.earscirev.2015.08.001>
- Yonkee, W. A., Weil, A. B., & Wells, M. L. (2024). Integrating structural, paleomagnetic, and thermo/geochronologic studies to understand evolution of the Sevier and Laramide belts, northern Utah to Wyoming. *Journal of Structural Geology*, 184, 105104. <https://doi.org/10.1016/j.jsg.2024.105104>
- Yoshimura, Y. (2022). The Cretaceous normal superchron: A mini-review of its discovery, short reversal events, paleointensity, paleosecular variations, paleoenvironment, volcanism, and mechanism. *Frontiers in Earth science*, 10, 834024. <https://doi.org/10.3389/feart.2022.834024>
- Zavala-Monsiváis, A., Barboza-Gudiño, J. R., Velasco-Tapia, F., & García-Arreola, M. E. (2012). Sucesión volcánica Jurásica en el área de Charcas, San Luis Potosí: Contribución al entendimiento del Arco Nazas en el noreste de México. *Boletín de la Sociedad Geológica Mexicana*, 64(3), 277–293.
- Zhou, Y., Murphy, M. A., & Hamade, A. (2006). Structural development of the Peregrina–Huizachal anticlinorium, Mexico. *Journal of Structural Geology*, 28(3), 494–507. <https://doi.org/10.1016/j.jsg.2005.11.005>
- Zijderveld, J. D. A. (1967). *AC demagnetization of rocks: Analysis of results, methods in Paleomagnetism* DW Collinson, KM Creer, SK Runcorn (pp. 254–286). Elsevier.